

# A Catalog of Visually Classified Galaxies in the Local ( $z \sim 0.01$ ) Universe

H. B. Ann<sup>1</sup> and Mira Seo<sup>1</sup>

Department of Earth Science, Pusan National University, Busan, Korea

and

D. K. Ha<sup>2</sup>

Youngdo High School, Busan, Korea

hbann@pusan.ac.kr

Received \_\_\_\_\_; accepted \_\_\_\_\_

Not to appear in Nonlearned J., 45.

## ABSTRACT

The morphological types of 5836 galaxies were classified by a visual inspection of color images using the Sloan Digital Sky Survey (SDSS) Data Release 7 (DR7) to produce a morphology catalog of a representative sample of local galaxies with  $z < 0.01$ . The sample galaxies are almost complete for galaxies brighter than  $r_{pet} = 17.77$ . Our classification system is basically the same as that of the Third Reference Catalog of Bright Galaxies with some simplifications for giant galaxies. On the other hand, we distinguish the fine features of dwarf elliptical (dE)-like galaxies to classify five subtypes: dE, blue-cored dwarf ellipticals, dwarf spheroidals (dSph), blue dwarf ellipticals (dE<sub>blue</sub>), and dwarf lenticulars (dS0). In addition, we denote the presence of nucleation in dE, dSph, and dS0. Elliptical galaxies and lenticular galaxies contribute only  $\sim 1.5\%$  and  $\sim 4.9\%$  of the local galaxies, respectively, whereas spirals and irregulars contribute  $\sim 32.1\%$  and  $\sim 42.8\%$ , respectively. The dE<sub>blue</sub> galaxies, which are a recently discovered population of galaxies, contribute a significant fraction of the dwarf galaxies. There seem to be structural differences between dSph and dE galaxies. The dSph galaxies are fainter and bluer with a shallower surface brightness gradient than dE galaxies. They also have a lower fraction of galaxies with small axis ratios ( $b/a \lesssim 0.4$ ) than dE galaxies. The mean projected distance to the nearest neighbor galaxy is  $\sim 260\text{kpc}$ . About 1% of local galaxies have no neighbors with comparable luminosity within a projected distance of 2Mpc.

*Subject headings:* catalog — galaxies: general — galaxies: statistics — galaxies: structure

## 1. Introduction

The morphology of galaxies is of great interest because it reflects not only the structural properties of galaxies but also their star formation histories. A morphological study of galaxies has been one of the main topics of extra-galactic studies since the pioneering work by Hubble (1936). Despite the enormous efforts to determine the morphological types of galaxies, the morphological types of the majority of galaxies from recent surveys, such as the Sloan Digital Sky Survey (SDSS), still need to be determined.

The morphology of bright galaxies in the local universe has been well studied and summarized in catalogs, such as A Revised Shaply-Ames Catalog of Bright Galaxies (RSA, Sandage & Tammann (1981)) and the Third Reference Catalog of Bright Galaxies (RC3, de Vaucouleurs et al. (1991)). However, none of these catalogs are suitable for dwarf galaxy studies because most dwarf galaxies which are much fainter than the bright end of dwarf galaxies are omitted due to their selection criteria. The recent study of Nair & Abraham (2010), who visually classified 14,000 SDSS galaxies from Data Release 4 (DR4), focussed on the redshift range  $0.01 < z < 0.10$ , and as a consequence included few dwarf galaxies. The Galaxy Zoo Project (Lintott et al. 2008) has provided morphological information for a much larger number of objects, but only in broad categories with little information on dwarf galaxies.

Dwarf galaxies, however, are predicted to be the most dominant type of galaxy based on cold dark matter (CDM) cosmology (White & Rees 1978). The importance of dwarf galaxies in galactic astronomy has been well demonstrated by the dominance of dwarf galaxies in the Local Group (LG), in which the number of dwarf galaxies tripled recently, mostly thanks to SDSS (McConnachie 2012; Walker 2013). They also dominate the nearby satellite systems such as those hosted by M81 (Chiboucas et al. 2009) and M106 (Kim et al. 2011). Galaxies with distances less than  $\sim 11\text{Mpc}$  and velocities relative to the LG

( $V_{\text{LG}}$ ) less than  $600\text{kms}^{-1}$ , which were compiled in the Updated Nearby Galaxy Catalog (Karchentsev et al. 2013a), are also dominated by dwarf galaxies. Makarov & Karachentsev (2011) presented an all-sky catalog of nearby galaxy groups that included 10,914 galaxies in the local universe ( $z \lesssim 0.01$ ) with various astrophysical parameters including the morphological types in numerical code  $T$ . On the other hand, they did not report the detailed morphological types of dwarf galaxies. Karchentsev et al. (2013a) provided a better treatment of the morphology of dwarf galaxies, but they confined the dwarfs to within  $\sim 11\text{Mpc}$ . Because galaxies in the local universe will provide a unique sample to explore the structural properties of dwarf galaxies, it is important to determine their detailed morphological types.

SDSS opens a new era of galaxy morphology by providing color images which are useful for obtaining information about the underlying stellar populations. Because stellar populations are closely related to the star formation history of galaxies, the morphological types that consider the stellar populations using color information and the light distributions can be considered to be the best proxy for characterizing the integral property of galaxies. The blue elliptical galaxy (Strateva et al. 2001), is an example of a new type of galaxy that has emerged in the new era of the galaxy morphology. Moreover, it is deep enough to cover dwarf galaxies as faint as  $M_r \approx -10$  in the local universe.

Another major difference between the morphological properties observed in single-band images and color images were found in the dwarf elliptical (dE) family. Although dE galaxies and dwarf spheroidal galaxies (dSph) are distinguished in the LG, they were used interchangeably for galaxies outside the LG in previous studies. In particular, Sandage & Binggeli (1984) used 'dE' and 'dE,N' for both dE galaxies and dSph galaxies in a classification of Virgo Cluster dwarfs, whereas Kormendy & Bender (2012) used Sph for both galaxies. On the other hand, there appears to be some difference between dE and

dSph (Weisz et al. 2011; McConnachie 2012). For example, dE galaxies are generally brighter and redder than dSph galaxies.

Although the environmental dependence of giant galaxies is well understood thanks to recent surveys, such as SDSS (Goto et al. 2003; Park et al. 2007), the dependence of dwarf galaxy morphology on environment has not been well studied due to the lack of dwarf galaxies in previous analyses. Therefore, it is important to produce a homogeneous sample of dwarf galaxies with detailed morphological types. Because the limiting magnitude of spectroscopic observations of the SDSS is  $r = 17.77$ , it is possible to make a volume-limited sample brighter than  $M_r = -15.2$  if galaxies with redshift less than  $z = 0.01$  are used. This provides an unprecedented opportunity to classify the morphological types of local galaxies using the color images of the SDSS DR7 with an emphasis on dwarf galaxies, whose morphological properties are still not well understood. Particular attention was paid to the morphologies of dE-like galaxies because they are the building blocks of larger structures in CDM cosmology. In particular, dSph are believed to be mostly dark matter dominated dwarfs (e.g., Gilmore et al. 2007). Because dE galaxies show different properties from dSph, such as the presence of gas and young stellar populations, at least for the LG dwarfs (Geha et al. 2010), it is important to determine whether they can be distinguished by morphology alone.

The aim of this paper is to perform a census of the morphology distribution of local galaxies brighter than  $M_r \approx -15$ . To accomplish this, the morphological types of all SDSS galaxies that have redshifts less than  $z = 0.01$  are classified by visual inspection of the color images of SDSS DR7. The results are presented in the form of a catalog that includes not only our classifications, but also numerical T types, adopted distances, absolute  $r$ -band magnitudes,  $u - r$  colors, and isophotal angular diameters and axis ratios. An additional aim is to better understand the environment of local galaxies, a factor which can play an

important role in morphology.

Section 2 introduces the observational data used in this study and the procedure for selecting the sample galaxies. Section 3 describes the methodology of morphology classification and Section 4 provides a catalog of the morphological types of the local galaxies. Section 5 presents the physical and morphological properties of the local galaxies and Section 6 reports the environmental dependence of the morphology. The final section provides a brief summary and discussion.

## 2. Sample

The basic sample of the local galaxies in this paper was derived from the Korea Institute for Advanced Study Value-Added Galaxy Catalog (KIAS-VAGC Choi et al. 2010), but was supplemented by galaxies with  $z < 0.01$  in the NASA Extragalactic Data Base (NED)<sup>1</sup> and the galaxies listed in Makarov & Karachentsev (2011) that are not overlapped with the galaxies from the KIAS-VAGC and NED. The KIAS-VAGC is a value-added catalog of galaxies based on the New York University Value-added Catalog (NYU-VAGC) DR7 which was derived from the SDSS DR7 (Abazajian et al. 2009)). the KIAS-VAGC provides valuable astrophysical parameters such as absolute magnitude and colors corrected for the galactic extinction as well as distances and morphological types determined by automated classifier (Park & Choi 2005). It also lists the redshifts of 10,497 galaxies that are not included in NYU-VAGC. They gathered redshift data from various catalogs (see Choi et al. (2010) for a detailed description). More detailed descriptions of SDSS data were reported by York et al. (2000) and Stoughton et al. (2002).

---

<sup>1</sup>NED is operated by the Jet Propulsion Laboratory, California Institute of Technology, under contract with the National Aeronautics and Space Administration.

All of the galaxies with redshifts less than 0.01 were selected from the KIAS-VAGC. The color images of the individual galaxies listed in the KIAS-VAGC were examined carefully to determine whether they are parts of a galaxy or multiply listed. A few tens of galaxies were removed from the selected galaxies because of their multiple entry or invalid redshift. The number of cleaned galaxies from KIAS-VAGC is 4807. In addition, 897 galaxies from NED, whose images and photometric data are available from SDSS DR7, were added. We present the number distribution of the sample galaxies as a function of redshift in Figure 1. The total number of sample galaxies is 5836.

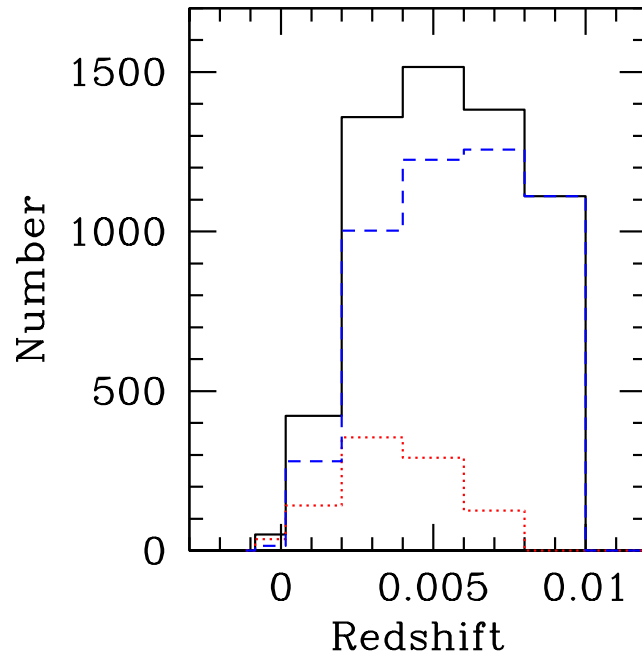


Fig. 1.— Number distributions of local galaxies as a function of the redshift. The dotted line indicates the galaxies in the Virgo cluster and the short dashed line represents the remaining galaxies. The entire sample of local galaxies is represented by the solid line.



Figure 2 shows the distribution of sample galaxies in a color-magnitude diagram. The Petrosian  $r$  magnitude and  $u - r$  color are used as the representative magnitude and color of a galaxy because the Petrosian  $r$  magnitude was used to select the spectroscopic target galaxies and the  $u - r$  color is one of the best proxies of the galaxy morphology because of its close dependence on the star formation rate (Strateva et al. 2001). Most galaxies brighter than the limiting magnitude of the SDSS spectroscopic target galaxies ( $r = 17.77$ ) are located in a relatively narrow range of  $u - r$  colors, whereas galaxies fainter than  $r = 17.77$  have a wide range of  $u - r$  colors. The color range of galaxies brighter than  $r = 17.77$  is similar to that of the volume-limited sample of galaxies brighter than  $M_r = -18.5$  (Choi et al. 2007). The redshifts of galaxies fainter than  $r = 17.77$  have been observed by other surveys, such as 2dFGRS (Colless et al. 2001), which is deeper than SDSS.

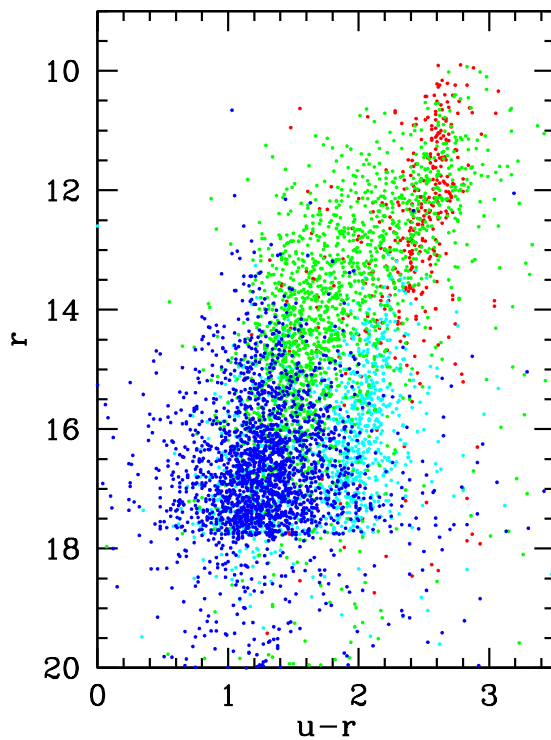


Fig. 2.— Color-magnitude diagram of the sample galaxies. The apparent Petrosian magnitude and  $u - r$  color are used. We distinguish galaxies with different morphology by assigning different color codes: red (ellipticals and lenticulars), cyan (dEs), green (spirals), blue (irregulars).

Figure 3 presents the distribution of  $r$ -band isophotal semi-major axis length ( $a$ ) and the axial ratio ( $b/a$ ) of sample galaxies whose isophotal semi-major and semi-minor axis lengths are available in the SDSS DR7. The isophotal axis lengths were measured at an isophote of  $25 \text{ mag arcsec}^{-2}$  at each pass-band. Most galaxies are larger than  $a_{iso} \approx 20$  pixels. Therefore, galaxies in the local universe ( $z < 0.01$ ) are large enough for visual classification. Approximately  $\sim 330$  spiral galaxies are inclined more than  $\sim 73^\circ$ . These edge-on galaxies comprise  $\sim 5\%$  of the total galaxies and  $\sim 20\%$  of spiral galaxies. Galaxies less than  $\sim 20 \text{ arcsec}$  are mostly face-on galaxies.

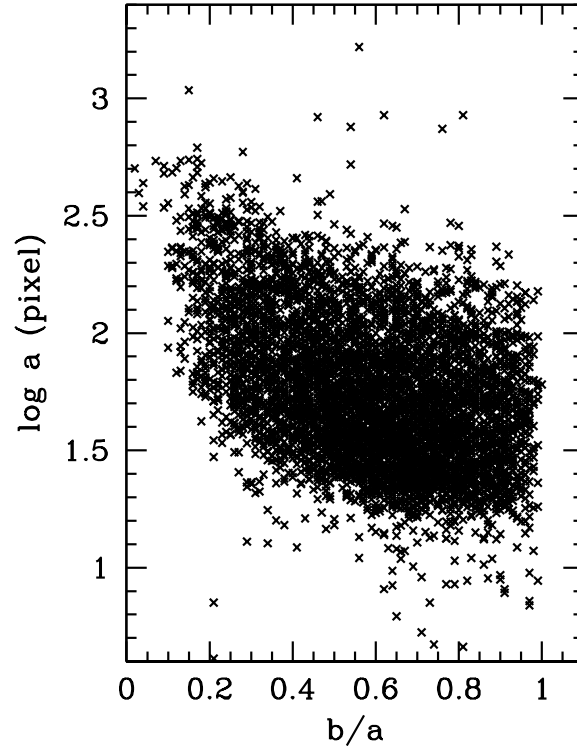


Fig. 3.— Semi-major axis and axial ratio of the sample galaxies. The  $r$ -band isophotal semi-major and semi-minor axes are used to derive axial ratios.

### 3. Morphology Classification

Traditionally, morphological classification has been performed through inspection of photographic plates or prints sensitive to the blue region of the spectrum (e.g., de Vaucouleurs 1959; Sandage 1961; Sandage and Tammann 1981; Sandage and Bedke 1994). More recently, galaxies have been classified using logarithmic, sky-subtracted digital  $B$ -band images in units of  $\text{mag arcsec}^{-2}$  (e.g., Buta et al. 2007). Therefore, in order to be "true" to the traditional classification systems, all of which are built on the original Hubble (1926, 1936) system, one should use SDSS  $g$ -band images since these are close enough in wavelength to the  $B$  band.

In the present study, however, we use the color images provided by the SDSS which are based on a combination of  $gri$  images (Lupton et al. 2004). For some galaxy types, the use of such images could lead to systematic differences from blue light classifications because the inclusion of the  $i$  band can enhance the prominence of galactic bulges, which play a role in the T type. Our reasons for using color images over  $g$ -band images are twofold. First, color adds information to morphology by its ability to distinguish underlying stellar populations. Second, our sample is dominated by galaxies that have very little or no bulge, making the possible impact of the  $i$  band on T types less of an issue. Park & Choi (2005) show that color gradients and the colors of galaxies are effective for automatic classification. We therefore feel that the use of color images for visual classification is justified.

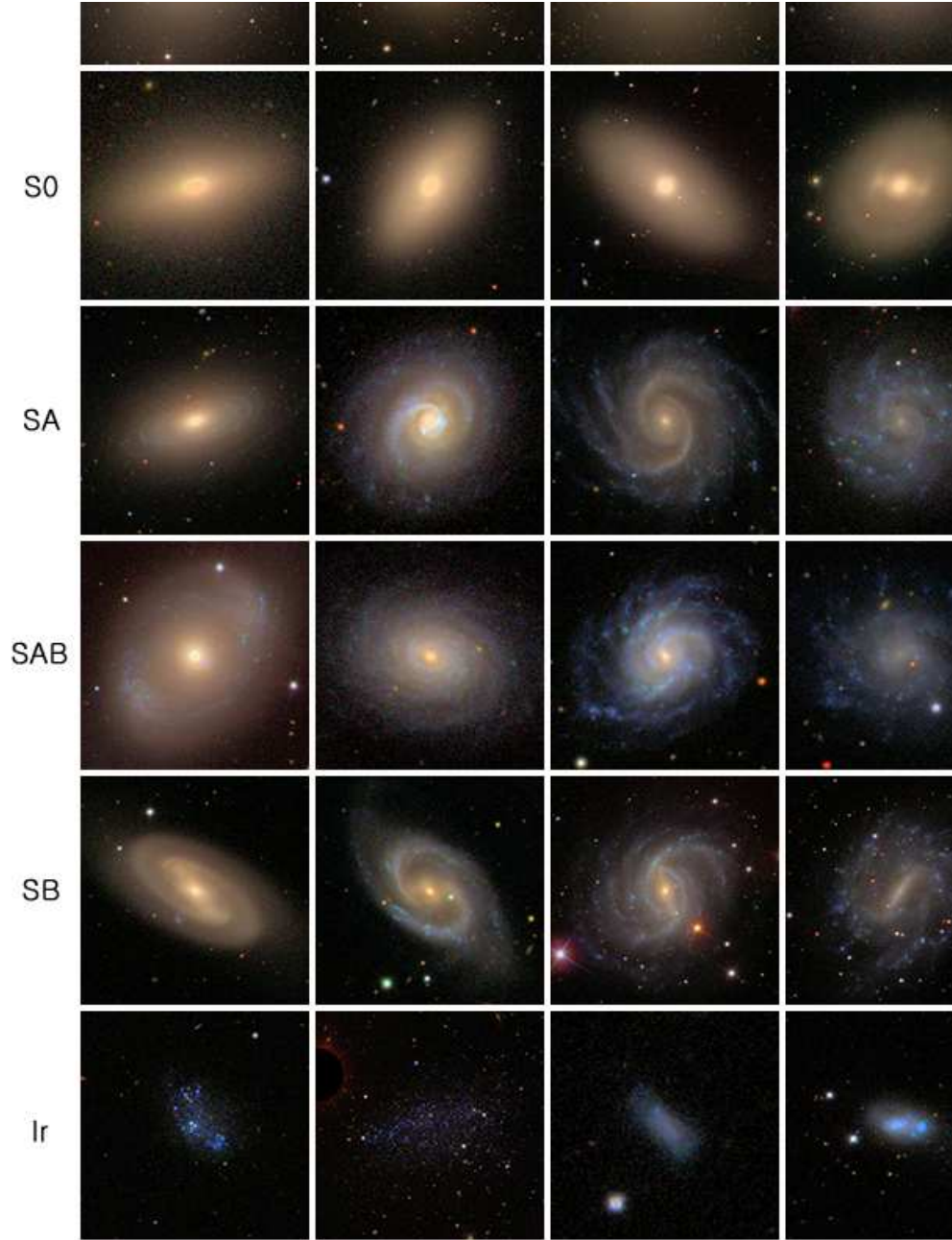


Fig. 4.— Sample images of E, S0, Sp, and Ir galaxies. Elliptical and lenticulars are in the first and second rows, respectively. Spirals grouped according to the bar types (SA, SAB, and SB) are displayed in the third, fourth, and fifth rows, respectively. Irregular galaxies, including BCDs are presented in the bottom row.

### 3.1. Methodology

The classification scheme of the morphological types of galaxies is based on the RC3 classification system (de Vaucouleurs et al. 1991), which is the de Vaucouleurs revised Hubble-Sandage system, or VRHS (de Vaucouleurs 1959). The description and sample color images given by Buta (2013) are also consulted. The classification scheme is simplified by neglecting stages of elliptical and lenticular galaxies. That is, the three stages of elliptical galaxies, compact ellipticals (cE), normal ellipticals (E), and late-type ellipticals ( $E^+$ ) and the three stages of lenticular galaxies,  $S0^+$ ,  $S0^0$  and  $S0^-$  are not distinguished. The reason for this is that these E/ $S0$  stages are based mostly on subtle aspects of structure and ignoring them has little impact on our analysis. On the other hand, all of the stages of spiral galaxies from 0/a to m are distinguished. dE/dSph galaxies are separated from giant ellipticals because the surface brightness distribution of dE galaxies is significantly different from that of the giant elliptical galaxies.

Elliptical galaxies are believed to have a simple structure. But, thanks to the color information that is sensitive to the underlying stellar populations, it is possible to detect peculiar morphologies induced by recent star formation in elliptical galaxies. The discovery of blue elliptical galaxies showing almost identical shapes to those of normal elliptical galaxies but with different colors (Strateva et al. 2001) is a good example of the usefulness of color images in extragalactic astronomy. Earlier studies of blue elliptical galaxies revealed anomalous blue cores (Michard 1999). For example, NGC 3156 and NGC 4742 have blue cores which are caused by the presence of young stellar populations in the nuclear regions (Michard 1999; Suh et al. 2010).

The distinction between elliptical galaxies and lenticular galaxies is made mainly by their surface brightness distribution. Elliptical galaxies show steeper surface brightness gradients than lenticular galaxies, particularly in the outer parts. This is why the

luminosity profiles of elliptical galaxies are best represented by the Sersic function with  $n \approx 4$  whereas those of lenticular galaxies are best fit by the Sersic function with  $n \approx 1$ . Galaxies with characteristics intermediate between ellipticals and lenticulars are classified as E/S0. Lenticular galaxies are further divided into three bar families, SA0, SAB0, and SB0, according to their bar types. The SA0 types show no bar feature, whereas the SB0 types show a clear bar morphology crossing the central bulge. Lenticular galaxies with intermediate bar types are assigned as SAB0. In the case of uncertain bar types, mostly due to high inclinations, they are classified as S0 galaxies.

For spiral galaxies, the spiral arm morphology is differentiated according to the Hubble stages adopted in RC3 (de Vaucouleurs et al. 1991). Namely, the stages, 0/a, a, ab, b, bc, c, cd, d, dm, and m, of spiral galaxies are determined according to the relative size of the bulge and the openness of the spiral arms. On the other hand, the spiral varieties, (r) and (s), are not distinguished because they are less fundamental than stage and family, and, as for the E/S0 stages, ignoring them has little or no impact on our analysis. We also exclude recognition of outer rings and pseudorings for the same reason. Therefore, for example, a strongly barred spiral galaxy with an intermediate Hubble stage is denoted as SBc, whereas a non-barred spiral galaxy with an intermediate Hubble stage is denoted SAc. For edge-on spirals, the bar families are not distinguished in this study and the Hubble stage is denoted as Sa, Sab, Sb, etc.

Irregular galaxies are divided into three types: Im, dwarf irregular (dI), and BCD. The first type, Im, is a natural extension of the late-type spirals and some Im galaxies are believed to have a bar component. In that case, a morphological type, IBm, is assigned. The second type, dI, represents small dwarf galaxies with an amorphous shape. Their physical properties, such as size, luminosity, and colors are similar to those of dSph and dE<sub>blue</sub> galaxies, which are described below. The last type, BCD, stands for the blue compact



dwarf and is characterized by star burst regions. They have amorphous shapes with high central surface brightness, and are likely to show an outer irregular envelope. However, there is no unique definition of BCD in the literature (Kunth & Ostlin 2000; Gil de Paz et al. 2003) but the morphological properties of BCDs in the present sample are similar to those of the BCDs analyzed by Gil de Paz et al. (2003). The shapes of BCD galaxies without an outer irregular envelope, i.e., HII region-like BCDs, are similar to the small blue dwarf elliptical galaxy ( $dE_{blue}$ ) described below. BCDs show an extremely blue color due to bursts of star formation. A significant fraction of irregular galaxies have small star burst regions. These galaxies are distinguished from Im and dI as well as BCD. We designate these galaxies as Ir/BCD.

In addition to dI galaxies, there are five types of dwarf galaxies: dwarf lenticular galaxies (dS0), dE galaxies, blue-cored dwarf elliptical galaxies ( $dE_{bc}$ ), dSph galaxies, and  $dE_{blue}$  galaxies. We designate these five dwarf galaxies as dE-like galaxies. The dwarf lenticular galaxies were introduced by Sandage & Binggeli (1984) for the morphological classification of dwarf galaxies in the Virgo cluster. They are characterized by lens-like features that have a shallow brightness gradient interior to a sharp edge. (See Buta (2013) for further discussion of lenses in disk galaxies.) In this respect, dS0 galaxies are different from their giant cousins, S0 galaxies, which are characterized by a bulge and a disk. A majority of dS0 galaxies show nucleation. The presence and absence of nucleation are distinguished by the subscripts 'n' and 'un' as  $dS0_n$  and  $dS0_{un}$  for a nucleated one and an un-nucleated one, respectively. Some dwarf galaxies exhibit similar characteristics to dS0 galaxies but the outer parts of these galaxies show disturbed disks, mostly resembling disrupted spiral arms. These galaxies are classified as  $dS0_p$ . We do not distinguish  $dS0_p$  galaxies from dS0 galaxies, except for the description of a detailed morphology.

dE galaxies can be distinguished from giant elliptical galaxies by their surface

brightness distribution, which is better represented by the Sersic function with  $n \approx 2$ . Most previous studies do not distinguish between dE galaxies and dSph galaxies (eg., Binggeli et al. 1985; Kormendy & Bender 2012). In particular, Kormendy & Bender (2012) use ‘Sph’ to represent spheroidal galaxies that can be placed in a position parallel to the Im galaxies in their revised parallel-sequence galaxy classification, which extends the van den Bergh parallel-sequence galaxy classification (van den Bergh 1976). They assumed that the Sph galaxies are stripped Scd-Im galaxies. However, our study considers dSph galaxies as a distinct population of dwarf galaxies because photometric properties, such as surface brightness and colors of dSph galaxies, seem to be different from those of dE galaxies. Moreover, if we consider that dSph galaxies are mostly dispersion-supported systems (Walker et al. 2009; Toloba et al. 2012) while a considerable fraction of dE galaxies are supported by rotation (Geha et al. 2010), their origins might be different.

The dE and dSph galaxies are distinguished by their surface brightness while  $dE_{blue}$  galaxies are distinguished from others by their blue color. The  $dE_{bc}$  galaxies are characterized by the presence of blue cores which are supposed to be regions of active star formation. The dE and dSph galaxies are further distinguished by their nuclear morphology:  $dE_{un}$ ,  $dE_n$ ,  $dSph_{un}$  and  $dSph_n$ . The distinction of nucleated dwarfs from un-nucleated dwarfs is somewhat arbitrary because the degree of nucleation varies continuously (Lisker 2009). Blue-cored dwarfs, however, are easily distinguished from nucleated dwarfs because the cores are bluer and larger than the nuclear region of nucleated dwarfs. Blue dwarf ellipticals ( $dE_{blue}$ ) have similar color to irregular galaxies. Their size is similar to or smaller than HII region-like BCDs. Small  $dE_{blue}$  and dI galaxies have similar features except for the axial symmetry. On the other hand, there is no clear distinction in the degree of axial symmetry for  $dE_{blue}$ . Therefore, it seems plausible that  $dE_{blue}$  galaxies are dI galaxies with an extreme axial symmetry.

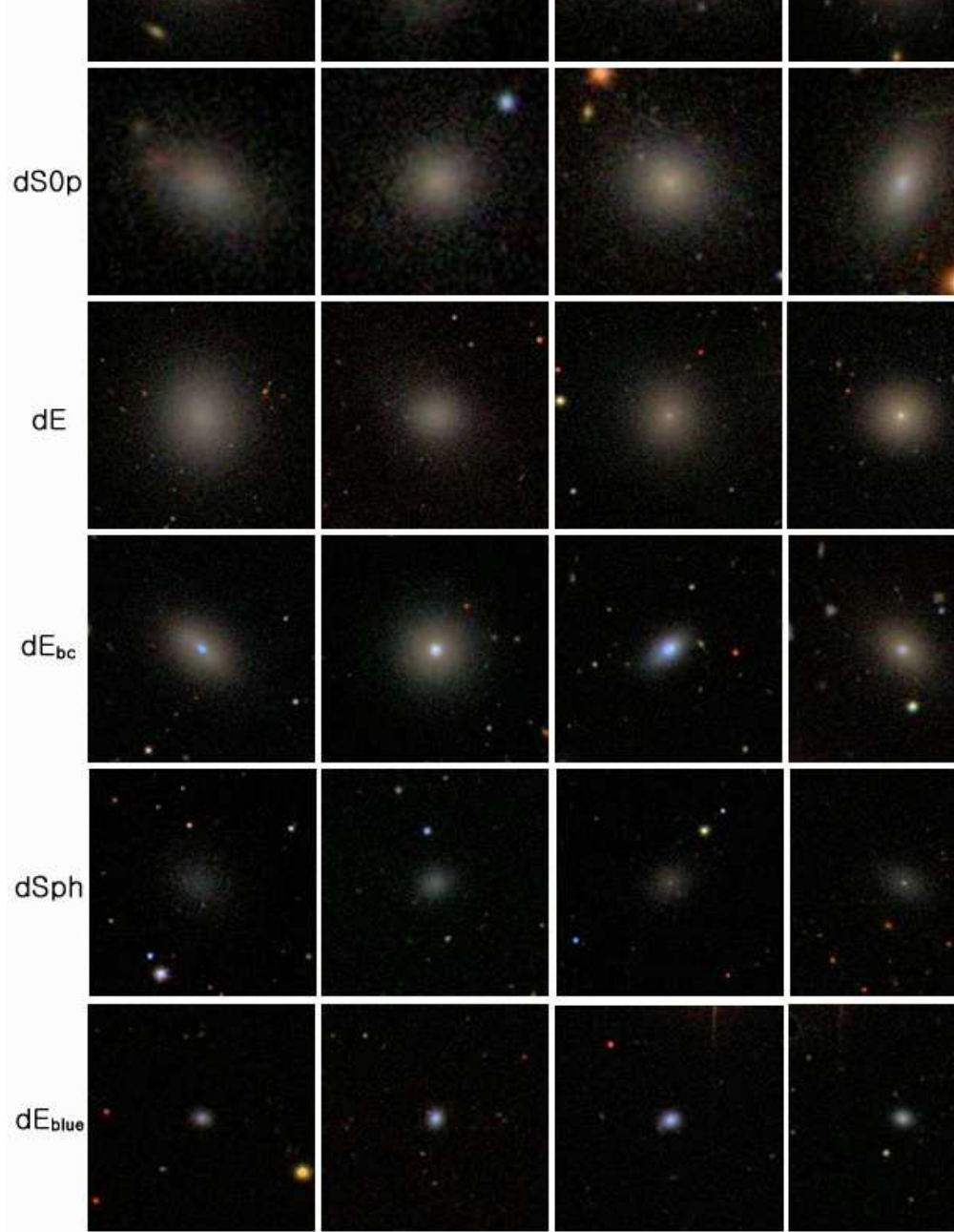


Fig. 5.— Sample images for dwarf elliptical-like galaxies: dS0 (first row), dS0<sub>p</sub> (second row), dE (third row), dE<sub>bc</sub> (fourth row), dSph (fifth row), and dE<sub>blue</sub> (sixth row).

For practical purposes, the numerical type  $T$  borrowed from RC3 is used with some simplification for the ellipticals ( $T=-5$ ) and lenticulars ( $T=-3$ ). However, we keep all of the Hubble stages from  $T=0$  to  $T=9$  for spirals (from  $0/a$  to  $m$ ) and  $T=10$  (Im) and  $T=11$  (dI) for irregulars. BCD is assigned as  $T=13$ , while irregulars containing small BCD-like components as  $T=12$ . Also, we assign new codes from -6 to -11 for dwarf elliptical-like galaxies:  $T=-6$  (dE),  $T=-7$  (dE<sub>bc</sub>),  $T=-8$  (dSph),  $T=-9$  (dE<sub>blue</sub>),  $T=-10$  (dS0, dS0<sub>p</sub>), and  $T=-11$  for transition type dwarf (dEs/dI dI/dEs), respectively.

In the present study, the color images of the sub-sample of galaxies were examined using the image display tool provided by the SDSS for training before the classification of the full sample of galaxies. The morphological types given in the NED were consulted during the training period. Because the number of subtypes to be classified is more than 20, morphological types were classified in two steps. Galaxies were divided into four broad types (elliptical/lenticulars, spirals, irregulars, and dE-like galaxies), and their fine subtypes were then classified after sorting the galaxies according to their broad types. The entire sample of galaxies was classified by each of the three authors. We followed two steps to finalize the morphological types of galaxies. In the first step, one of the authors (Seo) determined the morphological types of the entire sample by consulting the results of other authors. The final morphological type of each galaxy was determined by the senior author after reviewing Seo’s classification. There is not much difference between the final morphological types and those of Seo for giant galaxies (E, S0, and Sp) and irregular galaxies. However, about 10% of Seo’s classification of dE-like galaxies are revised, mostly within the category of dE-like galaxies.

### 3.2. Type Examples

Figure 4 shows representative images of elliptical, lenticular, spiral, and irregular galaxies classified in the present study. The elliptical and lenticular galaxies are displayed in the first and second rows, respectively. Spiral galaxies are presented in the third, fourth, and fifth rows, and are grouped according to the bar types (SA, SAB, and SB). The spiral galaxies are arranged according to the Hubble stage (a, b, c, d, and m) with the earliest types (SAa, SABa, and SBa) in the leftmost column and the latest types (SAm, SABm, and SBm) in the rightmost column. The irregular galaxies are presented in the sixth row. The first three columns present Im, dI, and Ir/BCD galaxies, respectively, whereas the fourth column and the fifth column display a BCD embedded in an irregular envelope and a BCD resembling HII regions, respectively. Different scales are used for each stamp image in Figure 4 for a better demonstration of their morphology.

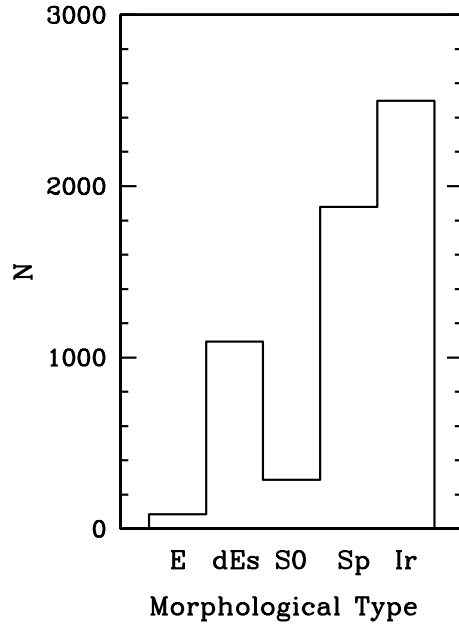


Fig. 6.— Morphology frequency of the 5836 galaxies within  $z = 0.01$ .

Figure 5 shows images of dE-like galaxies. The first and second rows display images of dwarf lenticular galaxies, with normal dwarf lenticulars (dS0) in the first row and dwarf lenticular galaxies with peculiar disk morphology (dS0<sub>p</sub>) in the second row. The morphology of dS0 galaxies is characterized by the presence of a lens-like feature in addition to the disk component. Lens-like features are normally redder than the disk but some dS0 galaxies have blue lens-like features due to young stellar populations near the nuclei. The galaxies in the third rows are dE galaxies. We arranged dE<sub>un</sub> galaxies in the first and second columns and dE<sub>n</sub> galaxies from third to fifth columns. In the fourth row, we display dE<sub>bc</sub> galaxies that show intense star formation in the nuclei of the galaxies. The nuclear star formation is thought to be caused by recent gas accretion (Sancisi et al. 2008; Kreckel et al. 2011). The fifth and sixth rows show dSph and dE<sub>blue</sub>, respectively. The dSph galaxies are generally fainter and bluer than the dE galaxies. Some dE<sub>blue</sub> galaxies have large blue cores, the radius of which is approximately half the galaxy size.

In addition to these types of galaxies, there are compact elliptical galaxies that are occasionally observed near the centers of clusters. They are smaller than the giant elliptical galaxies but their central surface brightness is similar to that of giant elliptical galaxies. Due to their high surface brightness, they are classified as compact elliptical galaxies rather than dE galaxies. A prototype of compact elliptical galaxies is M32 in the LG.

#### 4. Morphology Catalog of Local Galaxies

This section presents a catalog of the visually classified morphological types of 5836 galaxies whose redshifts are less than  $z = 0.01$ . The basic statistics of the morphological types of the local galaxies are reported along with a brief comparison with other studies. In addition, the new morphological types revealed from color images are briefly described.

#### 4.1. Catalog

The morphological types of 5836 galaxies are presented along with some basic data obtained from the SDSS DR7. Table 1 lists a part of the Morphological Catalog of Local Galaxies whose full content is available in the electronic version of this paper. The SDSS object identification number is used as the name of a galaxy but the primary NED name is presented in the last column for reference. This paper uses the distance of a galaxy derived from the heliocentric redshift corrected for the motion of the LG. We used the prescription of Mould et al. (2000) to derive the velocity relative to the centroid of the LG ( $V_{LG}$ ). On the other hand, for those galaxies lying inside a  $10^\circ$ -cone around M87 with a heliocentric redshift less than  $z=0.007$  (Kraan-Korteweg 1986), the distance of the Virgo cluster is used. A Hubble constant of  $H=75\text{kms}^{-1}$  was used. The catalog contains 12 columns with the following information.

Column 1: SDSS Object ID.

Column 2: Right ascension (J2000.0) in degrees.

Column 3: Declination (J2000.0) in degrees.

Column 4: Heliocentric redshift determined by spectroscopic observations

Column 5: Morphological types determined in the present study.

Column 6: Morphological index  $T$ . The  $T$  code is adopted from RC3 but somewhat simplified except for spirals. We add new codes to distinguish subtypes of dwarf galaxies (see section 3.1 for the description of  $T$  code).

Column 7: Distance in Mpc derived from the radial velocity relative to the LG.

Column 8: Absolute magnitude in the  $r$ -band ( $M_r$ ). We use the model magnitude from SDSS DR7 corrected for the galactic extinction (Schlegel et al. 1998). The SDSS model magnitude is a magnitude derived by best-fitting model (exponential profile or de Vaucouleurs profile) to the observed images.



Column 9: Model  $u - r$  color (extinction corrected)

Column 10: Isophotal semi-major axis in pixels measured at  $\mu_r = 25 \text{ mag arcsec}^{-2}$

Column 11: Isophotal axis-ratio

Column 12: Galaxy names in the literature. The first entry in NED is taken. In cases of no NED name, we make a name using the coordinates of the galaxy similar to the SDSS object name.

Table 1. Catalog of the morphological types of local galaxies.

ID	RA	DEC	z	Morphology	T	D (Mpc)	$M_r$	$u - r$	$a_{iso}$	$(b/a)_{iso}$	name
587731514215760014	17.283075	1.121029	0.003855	dI	10	17.5	-14.79	0.73	44.7	0.5	SHOC053
588015510351118339	18.232364	0.981506	0.003843	SABdm	8	17.43	-18.79	1.86	-9	-9	NGC0428
588015510351184046	18.413968	0.875452	0.003873	Sm/Im	10	17.55	-13.73	0.69	26.2	0.71	UGC00772
588015510351249607	18.584742	0.916687	0.003717	dI	10	16.92	-14.77	1.05	41.4	0.5	SDSSJ011420.41+005503.2
588015507666960497	18.719523	-1.095353	0.006761	dS0n	-10	29.05	-16.02	1.45	40.4	0.62	SDSSJ011452.68-010543.2
587743981974650974	18.84512	8.099593	0.007812	SAcd	6	33.24	-17.09	2.39	61.4	0.74	UGC00803
587731511532060697	18.876839	-0.86098	0.005874	SABcd	6	25.51	-18.95	1.54	149.1	0.77	NGC0450
587731511532191838	19.087214	-0.911365	0.005576	dI	10	24.32	-15.12	1.07	26.9	0.85	SDSSJ011620.92-005440.8
758877280840910682	19.106185	33.431996	-0.000627	dSphun	-8	0.64	-10.52	2.62	4.7	0.74	AndII
758877278149148728	19.18239	16.400064	0.006615	SAa	1	28.46	-18.74	1.74	88.2	0.76	CGCG459-021
587727226772258858	19.377137	-9.296768	0.006479	SAm	9	27.91	-16.47	1.11	73.9	0.37	SDSSJ011730.51-091748.3
587727179531747451	19.809026	-9.597428	0.006379	Im/BCD	12	27.5	-14.81	1.16	29.5	0.43	SHOC061
587731512606326893	20.028347	-0.205448	0.00581	Sdm	8	25.23	-17.18	1.52	106.6	0.29	UGC00866
588015510351970406	20.26232	0.851495	0.008134	dI	10	34.48	-15.83	1.02	24.4	0.69	SDSSJ012102.95+005105.3
587744045327319127	20.364876	7.018498	0.007495	Sa	1	31.94	-19.3	1.65	111	0.39	NGC0485
588015509278359598	20.522909	0.08518	0.007569	SAdm	8	32.23	-15.84	1.58	77.8	0.14	FGC0156
588015510352101409	20.537435	0.945465	0.007799	Scd	6	33.14	-19.91	1.92	310.6	0.19	NGC0493
588015508204748937	20.810885	-0.700637	0.006625	Sd	7	28.46	-16.83	1.38	88.3	0.23	UGC00931
587743980364955756	20.93191	6.691629	0.007789	SABcd	6	33.09	-17.14	1.74	50.7	0.96	UGC00942

Note. — Table 1 is published in its entirety in the electronic edition of the *Astrophysical Journal Supplement*. A randomly selected portion is shown here. Color images of the galaxies listed in Table 1 are provided in the web (<http://earth.es.pusan.ac.kr/hbann/apjs/z01image>).

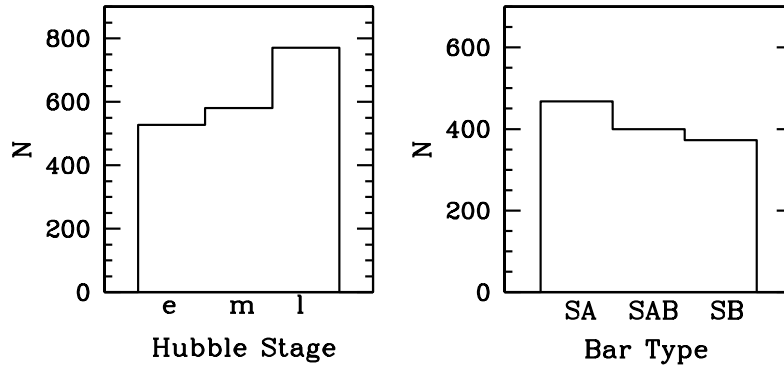


Fig. 7.— Frequency of spiral galaxies as a function of the Hubble stage (early (e), intermediate (m), and late (l)) in the left and frequency of spiral galaxies as a function of the bar type (SA, SAB, and SB) in the right.

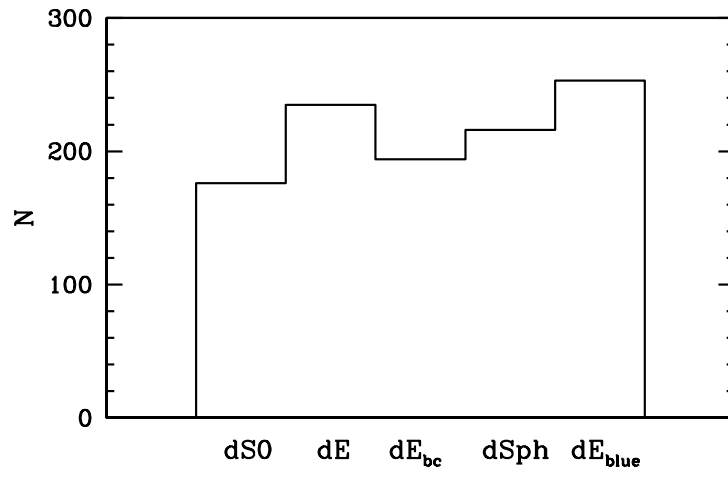


Fig. 8.— Frequency of subtypes of dwarf elliptical-like galaxies (dEs).

Table 2. Frequency of the morphological types of local galaxie

	E	dEs	S0	Sp	Ir
number	86	1092	286	1878	2498
fraction	0.015	0.187	0.049	0.321	0.428

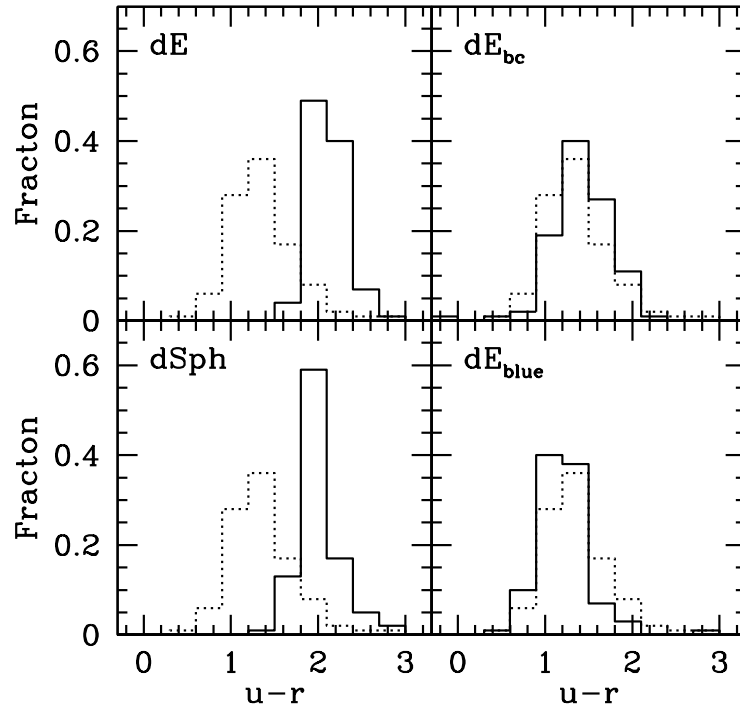


Fig. 9.— Color distributions of dwarf galaxies: dE, dE<sub>bc</sub>, dSph and dE<sub>blue</sub>. The histograms plotted by dotted lines represent dI galaxies.

## 4.2. Frequency Distributions of Morphological Types

Figure 6 presents the frequency distribution of the broad morphological types of 5836 galaxies. Irregular galaxies are most abundant (42.8%), and spiral galaxies are second-most abundant (32.1%). These two types comprise  $\sim 75\%$  of the local galaxies. The fractions of elliptical galaxies and lenticular galaxies are 0.015 and 0.049, respectively. The fraction of dE-like galaxies is 0.187. If we exclude the dS0 galaxies, it becomes  $\sim 0.15$ . Therefore, they are 10 times more frequent than their giant cousins, elliptical galaxies. The local universe is dominated by dwarf galaxies because the majority of irregular galaxies are dwarf galaxies. Table 2 lists the basic statistics of the morphological types of galaxies presented in this catalog (Table 1).

Figure 7 shows the frequency of the Hubble stages (top panel) and that of the bar family (bottom panel). The Hubble stages are grouped into three stages of early (e), intermediate (m), and late (l). The edge-on galaxies are included in the frequency distribution of the Hubble stages but they are not included in the frequency distributions of the bar family. The number of spirals increases from the early types to the late types. The fraction of barred galaxies (SAB and SB) is  $\sim 0.62$  which is similar to the bar fraction in RC3 (de Vaucouleurs et al. 1991) and that derived from the mid-IR images of nearby galaxies (Buta et al. 2015) but somewhat higher than those derived from the SDSS galaxies at  $z > 0.01$  (Lee et al. 2012; Oh et al. 2012; Skibba et al. 2012). The bar fraction from the ellipse fitting technique (e.g., Barazza et al. 2009) is somewhat lower than the visual classifications but that from Fourier analysis (Kraljic et al. 2012) is somewhat higher than that in the present study. The difference in the bar fractions is due mostly to the classification method and the criteria for bar selection. The lowest bar fraction from the SDSS data is that derived by Oh et al. (2012) who reported a bar fraction of 0.36.

Figure 8 shows the frequency distribution of the subtypes of dE-like galaxies; dE, dE<sub>bc</sub>,

dSph, dE<sub>blue</sub>, and dS0. As shown in Figure 8, the dominant population of the dE-like galaxies is dE<sub>blue</sub> galaxies, which is distinguished from the others by its blue color. The second largest population is dSph galaxies, but if dE<sub>bc</sub> galaxies are considered to be a special type of dE, then the number of dE is similar to that for dSph. The dS0 galaxies include dS0<sub>p</sub> galaxies which show signatures of spiral arm structures in the outer parts.

Figure 9 shows the frequency distributions of  $u - r$  colors for the subtypes of dE-like galaxies with those of dI for comparisons. The dE galaxies show the reddest color with narrow color ranges, whereas the dE<sub>blue</sub> galaxies show the bluest color similar to that of dI galaxies. The dSph galaxies show redder colors than dE<sub>bc</sub> and dE<sub>blue</sub>. Their average color is similar to that of dE galaxies but they have a  $u - r$  color distribution extended to blue colors up to  $u - r \approx 1$ .

### 4.3. Comparison with Others

This classification is compared with the automated classification (Park & Choi 2005) given in KIAS-VAGC. Because they presented broad morphological types (early and late types) only, the types in this study were also grouped into early and late types. The early type includes ellipticals (E) and lenticulars (S0) with their dwarf cousins (dE, dE<sub>bc</sub>, dSph, dE<sub>blue</sub>, and dS0) and the late type includes spirals (Sp) and irregulars (Ir). Spiral galaxies show the best match (94%) and dE-like galaxies show the worst match (44%) between the present classification and that reported by Park & Choi (2005). Ellipticals (E) and irregulars (Ir) also show good matches of  $\sim 90\%$ , whereas lenticulars show fair matches (73%). The low match between the present classification and Park & Choi (2005) for dE-like galaxies is due mostly to the extremely high mismatch of dE (dE<sub>un</sub> and dE<sub>n</sub>) and dSph (dSph<sub>un</sub> and dSph<sub>n</sub>), which show only 30% matches. For both dE and dSph, the un-nucleated ones show better matches. The worst match was found for nucleated dwarf



spheroidals ( $\text{dSph}_n$ ) which showed only a 24% match. On the other hand,  $\text{dE}_{bc}$  and  $\text{dE}_{blue}$  show the  $\sim 60\%$  matches. The reason for the worse classification of dE and dSph galaxies appears to be the small number of dwarf ellipticals in the training sample of Park & Choi (2005). In the case of  $\text{dE}_{bc}$  and  $\text{dE}_{blue}$  galaxies, they included a sufficient number in their training sample.

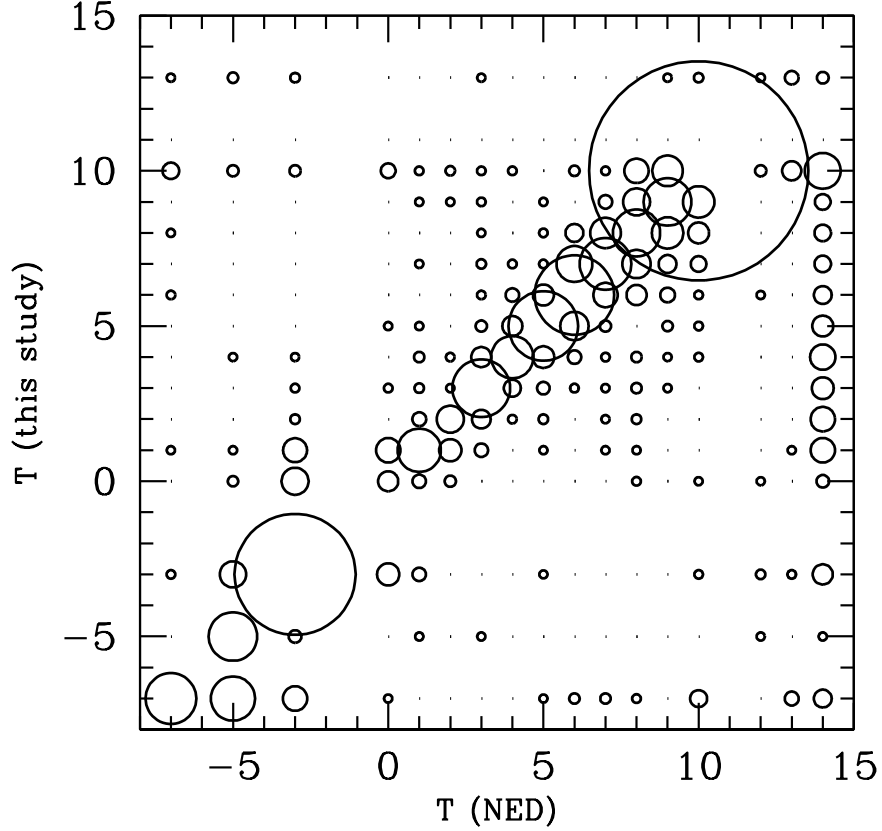


Fig. 10.— Comparisons of morphological types determined by the present study and those in the NED. We use the same numerical code  $T$  as those in RC3 for spiral galaxies ( $T=0$  to  $T=9$ ). Ellipticals and lenitculars are coded as  $T=-5$  and  $T=-3$ , respectively. The dwarf elliptical-like galaxies are coded as  $T=-7$  and irregulars (Im, dI, and Ir/BCD) are coded as  $T=10$  and BCDs as  $T=13$ . In addition,  $T=12$  is assigned to I0 galaxies and  $T=14$  for spirals with unknown stages.

Figure 10 compares the morphological types determined in this study with those from NED. We use the numerical type  $T$  adopted in the present catalog with three additional codes:  $T=12$ ,  $T=13$ , and  $T=14$ . The first and second ones are used for the NED I0 galaxies and BCD galaxies, respectively. The last one is assigned to the spiral galaxies with no Hubble stage. They are usually given as S? or SB?, which suggests an uncertain morphology. In addition to these types,  $T=-7$  is assigned to dE-like galaxies. The circle sizes in Figure 10 are proportional to the fractions of the types classified in the present study. As shown in Figure 10, there is good agreement between the present types and those from the NED. On the other hand, there are two types that show a considerable difference. One type is elliptical galaxies ( $T=-5$ ) and the other is I0 galaxies ( $T=12$ ). Some bias in the classification of S0/a galaxies can be seen. The NED S0/a galaxies ( $T=0$ ) are classified mainly as one of the three types, S0, S0/a, and Sa. If the S0/a is highest, as in Figure 10, then the Sa fraction would be slightly higher than the others.

For elliptical galaxies, approximately half of the NED ellipticals are classified as lenticulars or dE-like galaxies in the present study. This is expected because there is frequent confusion between elliptical and lenticular galaxies in the literature. Note that most NED lenticular galaxies are classified as lenticular galaxies, whereas NED elliptical galaxies are classified frequently as lenticular galaxies. The confusion between ellipticals and dE-like galaxies is also conceivable because they differ only in the surface brightness and its gradient. As shown in Figure 10, ellipticals are more likely to be misclassified as dwarf ellipticals/spheroidals than lenticulars.

I0 is a special type of irregular galaxy. It is not so irregular because it is not as disorganized, which is the main characteristics of irregular galaxies. I0 galaxies show a smooth structure similar to lenticular galaxies but have central irregular zones of active star formation (Buta 2013). This type is not included as a separate class because they

do not have properties that can be easily distinguishable from other types of galaxies. Recent observations show that many elliptical/lenticular galaxies show similar features in their central regions. As expected, most I0 galaxies are classified in the present study as either lenticular galaxies ( $T=-3$ ) or irregular galaxies ( $T=10$ ). **In the mid-IR, I0s like NGC 2968, 3077, and 5195 are much more regular and the class is no longer applicable (Buta et al. 2015).**

A considerable difference between the present types and NED types can also be observed in BCD galaxies ( $T=13$ ). Most of our BCDs are also classified as BCDs in NED. However, the majority of NED BCDs are classified as irregulars ( $T=10$ ). This is due to those Ir/BCD galaxies which are considered as irregular galaxies in our classification but most of which are classified as BCDs in NED. Confusion with irregular galaxies is natural because many irregular galaxies have star burst regions, which is a basic characteristic of BCDs. Such irregular galaxies are considered to be BCDs in the present study only if the star burst regions are large enough to dominate the luminosities of galaxies. The introduction of  $dE_{blue}$  galaxies is another cause of the large mismatch between the NED BCDs and our types for these galaxies. Similar fractions of NED BCDs are classified as BCDs and  $dE_{blue}$  galaxies in our classification. Some  $dE_{blue}$  galaxies are small enough, i.e., comparable to HII region-like BCDs with similarly blue color with the BCD color.

The circles at  $T=-7$  represent early-type dwarf galaxies. They are not divided into subtypes of dE,  $dE_{bc}$ ,  $dE_{blue}$ , dSph, and dS0 because the NED types were not finely defined. Most NED early-type dwarfs are classified by us as early-type dwarfs but a small fraction of NED early type dwarfs are classified as irregular galaxies. A better comparison of early-type dwarfs with others is given below (Figure 13). Finally, the small circles at  $T=14$  represent spiral galaxies with no Hubble stages in NED. Most spiral galaxies we classify as spirals but some are classified as lenticulars, early-type dwarfs, irregulars, and BCDs.

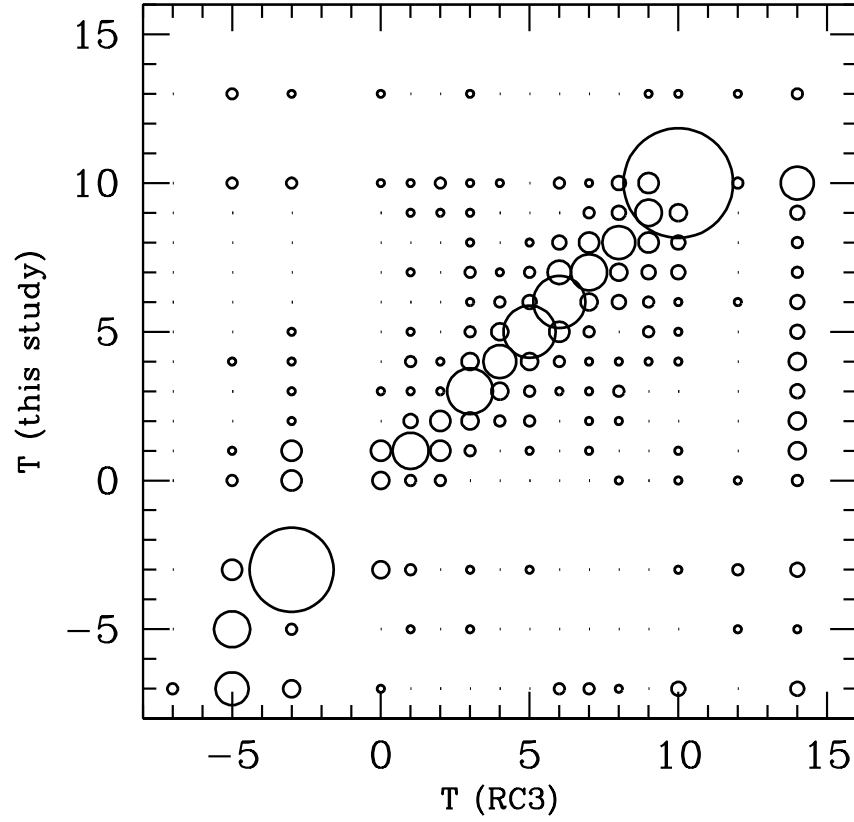


Fig. 11.— Comparisons of morphological types determined by the present study and those in the RC3. The  $T$  codes are the same as those in Figure 10.

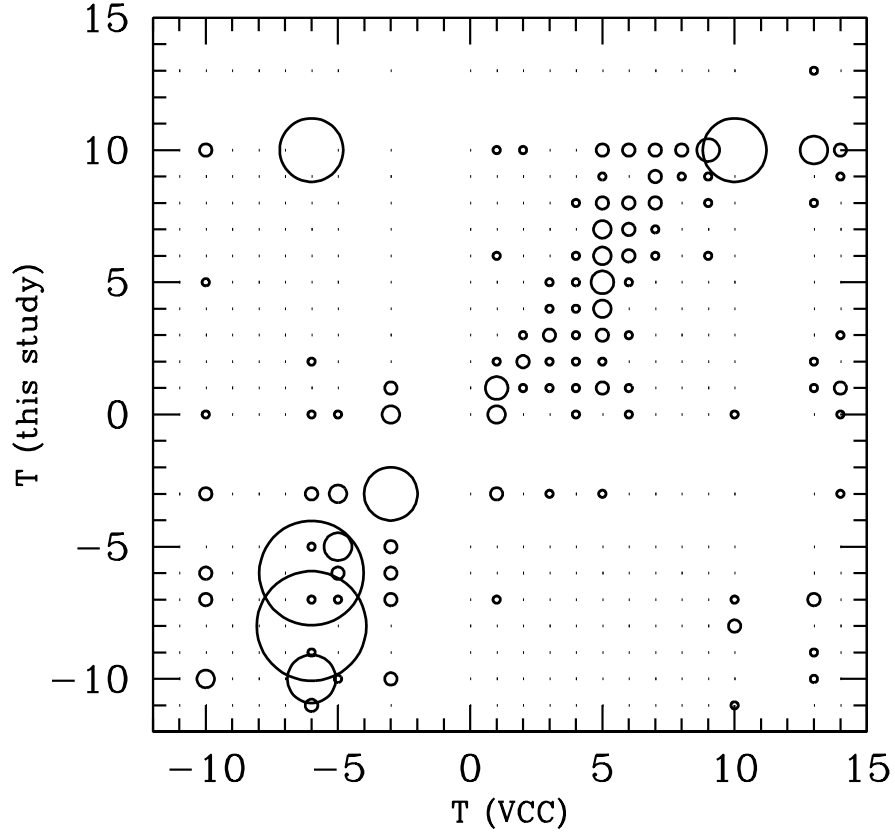


Fig. 12.— Comparisons of morphological types determined by the present study and those in the VCC. The  $T$  (VCC) codes are the same as  $T$  (NED) in Figure 10 except for  $T$  (VCC)=-6 and  $T$  (VCC)=-10 which are assigned to dEs and dS0, respectively.

Figure 11 compares the present types with those of RC3 (de Vaucouleurs et al. 1991). We used the same convention of  $T$  type. As shown in Figure 10 and Figure 11, the two comparisons are very similar. This similarity is due to the fact that most of the NED types come from RC3. For the galaxies in the present catalog, 95% of NED types come from RC3. The absence of galaxies at  $T$  (RC3)=13 is due to the lack of BCD types in RC3. There are 18 galaxies whose morphological types are classified as peculiar galaxies (P) in RC3. The majority of these galaxies are classified as irregulars (7 galaxies) and BCDs (5 galaxies). The remaining 6 galaxies consist of four spirals, one lenticular galaxy, and one dE galaxy.

Figure 12 shows the comparison of the morphological types with those in the Virgo Cluster Catalog (Binggeli et al. 1985, hereafter VCC). Since in VCC, dS0 galaxies are distinguished from other dE-like galaxies, we assign  $T$  (VCC)=-6 to dEs and  $T$  (VCC)=-10 to dS0 in Figure 12. However, we keep our subtypes of dE (-6), dE<sub>bc</sub> (-7), dSph (-8), dE<sub>blue</sub> (-9), dS0 (-10), and dEs/dI (-11) in Figure 12 to see how VCC dEs distribute in our dE-like galaxies. For the types from  $T$ =-5 to  $T$ =14, we used the same conventions as those in Figure 11. As shown in Figure 12, there is a fairly good agreement between the morphological types determined in this study and those in VCC. However, the degree of agreement is worse than RC3, especially for the Hubble stages of spiral galaxies later than  $T$  (VCC)=3. The best agreement between this study and VCC is observed for lenticular galaxies. Elliptical galaxies also give quite good agreement. On the other hand, the greatest discrepancy between this study and VCC is observed for VCC BCDs. The majority of VCC BCDs are classified as irregulars in this study. There are two dwarf spiral galaxies in VCC. One is IC 3094, which is given a type of ‘dS?’. The NED type of this galaxy is ‘S; BCD’ and we classified it as ‘SAa’. The other is NGC 4192 which is classified as ‘d:Sc’ in VCC. We classified it as ‘SAcd’ while NED gives ‘SAB(s)ab’.

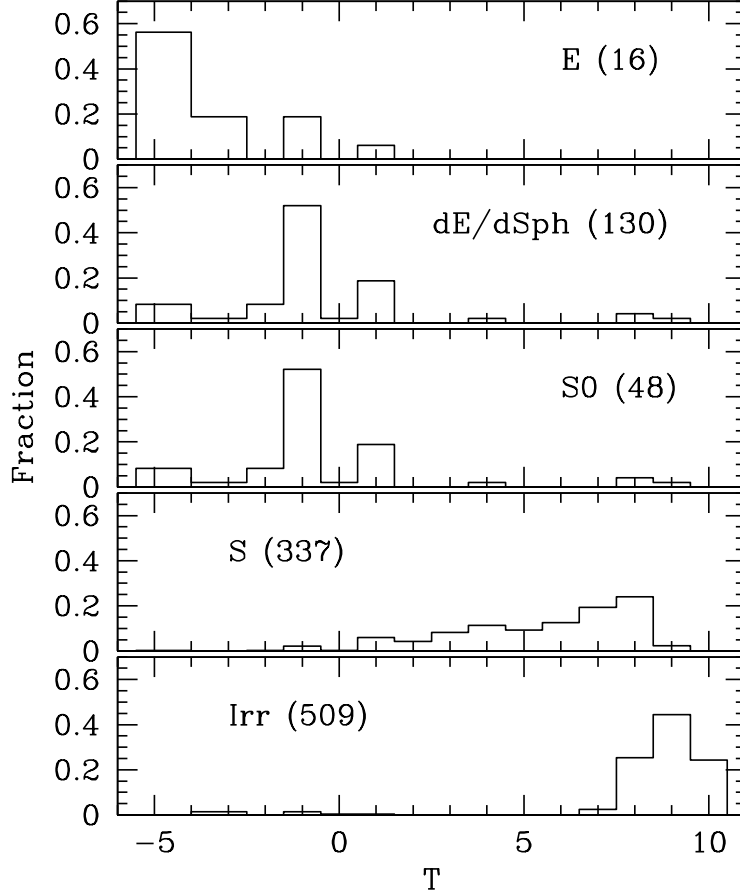


Fig. 13.— Comparison of present morphological types and those in the KN. We use the numerical code  $T$  of Karchentsev et al. (2013a):  $T=-3$  (dSph),  $T=-2$  (dE),  $T=-1$  (S0), and  $T=0$  (dS0). From  $T=1$  to  $T=8$  are assigned to spirals as  $T=1$  for Sa and  $T=8$  for Sdm and Sm. Irregulars including BCDs are assigned as  $T=9$  and transition types as  $T=10$ .



Figure 13 compares the types in this study with those reported by Karchentsev et al. (2011, 2013a,b,c, 2014). These studies (KN hereafter) include the Updated Nearby Galaxy Catalog. We plot the fractional distributions of the morphological types of galaxies in the KN that are listed in our catalog. Our morphological types are grouped into five broad types E, dEs, S0, Sp, and Ir, and we display the fractional frequency distributions of  $T$  in KN at each panel, which are labeled according to morphological type with the number of galaxies in parentheses. The  $T$  codes adopted by Karchentsev et al. (2013a), which are slightly different from the  $T$  codes used in the present catalog, are used for convenience.

The elliptical galaxies are presented in the top panel. There are only 16 shared galaxies, 9 of which are classified as ellipticals in KN while all of the other galaxies except one (MCG-01-33-007) are classified as dEs or lenticulars. The type  $T=-2$  and  $T=-3$  were assigned for dE and dSph, respectively, in KN. The second panel shows the fractional distribution of the morphological types of galaxies classified as dE-like galaxies in our catalog. Our dwarf galaxies designated as dEs include dE, dE<sub>bc</sub>, dSph, dE<sub>blue</sub>, and dS0s. Here, we present here 131 dEs that are shared with KN. As shown in the second panel of Figure 13, there is a significant disagreement in the morphological types between ours and those of KN. Among 130 dEs, 18 galaxies are classified as irregular galaxies and 42 galaxies as spirals, which are mostly late-types of stages dm and m ( $T=8$ ). The third panel from the top in Figure 13 shows 48 lenticulars listed in the present catalog, which show a wide range of  $T$  in Karchentsev et al. (2013a). About 53% of our lenticular galaxies are classified as  $T=-1$ , which is assumed to designate lenticular galaxies in KN. Among the 22 galaxies that were not classified as lenticulars in KN, 4 galaxies are ellipticals and 5 are dEs. In particular, 10 galaxies that correspond to 20% of the S0 galaxies are classified as early-type spirals of stage 0/ $a$  and  $a$ . The fourth panel from the top shows the fractional distribution of the KN morphological types for our spiral galaxies. There is a good agreement between the current classification and those in KN. The fraction of spirals with  $T > 4$  is 65%, which

is in good agreement with that of the present catalog (64%). As shown in the bottom panel of Figure 13, most of irregular galaxies ( $\sim 95\%$ ) are classified as  $T=8$ ,  $T=9$ , and  $T=10$  in the KN where late-type spiral galaxies (dm and m), irregulars including BCDs, and transition types are classified as  $T=8$ ,  $T=9$ , and  $T=10$ , respectively.

## 5. Properties of Local Galaxies

### 5.1. Luminosity and Color

The absolute  $r$ -band magnitude and  $u - r$  color are basic properties of a galaxy. The former is related directly to the mass of a galaxy, which is the most important parameter in the formation and evolution of the galaxy, whereas the latter is closely related to the star formation history. Because most of the sample galaxies do not have redshift-independent distances, we use redshift-dependent distances for all of them to calculate  $M_r$ . We corrected the motion of the LG following (Mould et al. 2000) but the K-correction and evolution correction are not applied in the derivation of  $M_r$  because they are negligibly small for local galaxies.

Figure 14 shows the  $u - r$  color versus  $M_r$  diagram of the 5836 galaxies listed in the present morphological catalog. Some features should be noted. First, galaxies with a different morphology occupy different parts of the color-magnitude diagram. The so called red sequence is well defined from  $M_r \approx -13$  to  $M_r \approx -22$  within which the luminosity-color relationship is well established. The upper part of the red sequence consists of elliptical galaxies and S0 galaxies (red color), whereas the lower part consists of dE-like galaxies (cyan color). They overlap around  $M_r \approx -17$ , which suggests that  $M_r = -17$  is the bright limit of dwarf galaxies. Second, irregular galaxies (blue color) display the blue cloud. They are clustered around the mean values of  $M_r = -14.5 \pm 3.3$  and  $u - r = 1.36 \pm 0.42$ ,

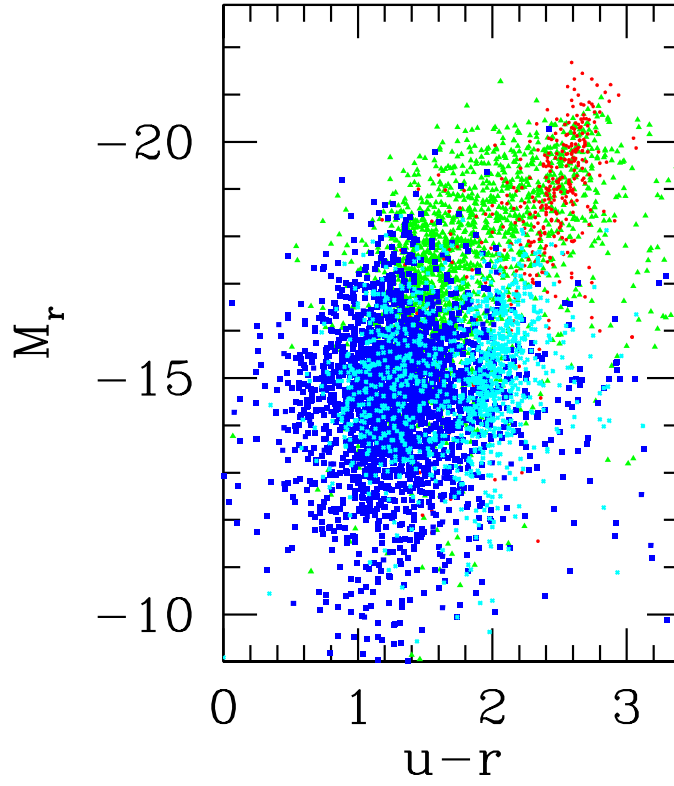


Fig. 14.— Color-magnitude diagram of the local galaxies. Filled triangles, filled rectangles, and crosses represent spirals, irregulars, and dwarf elliptical-like galaxies, respectively, whereas solid dots designate ellipticals and lenticulars.

respectively. Some dE-like galaxies are located in the blue cloud. They are mostly dE<sub>blue</sub> galaxies. Third, spiral galaxies are located mostly in the green valley. The majority of spiral galaxies are brighter than the dwarf limit of  $M_r = -17$  but a non-negligible fraction of spiral galaxies are fainter than  $M_r = -17$ . This is due mainly to the late-type spiral galaxies of the Hubble stages d, dm, and m. Finally, there are a number of galaxies whose photometry needs to be refined. For example, galaxies located in the far red envelope of the red sequence are probably due to poor photometry, even though some are due to heavy extinction. In addition,  $M_r$  of galaxies fainter than  $M_r = -10$  are also due mostly to poor photometry.

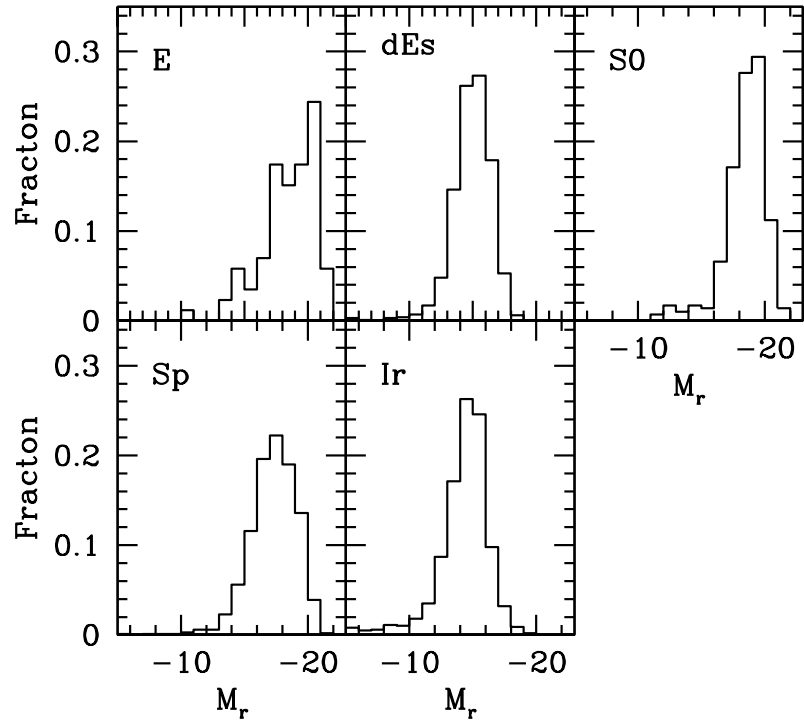


Fig. 15.— Fractional frequency distributions of  $M_r$  of the local galaxies. The 'dEs' represents the dwarf elliptical-like galaxies.

Figure 15 shows the fractional frequency distributions indicating the luminosity distribution of local galaxies. The galaxies are grouped according to their broad morphological types: E, dEs, S0, Sp, and Ir. Although HII region-like BCD galaxies are supposed to be dwarf galaxies similar to  $dE_{blue}$ , we grouped all the BCDs as a subtype of the Ir class because the majority of BCD components are imbedded in the irregular galaxies. Luminosity distributions of galaxies with different morphological types differ significantly. Elliptical galaxies show a highly asymmetric distribution that peaks at  $M_r = -20.5$ , whereas dEs and irregular galaxies show symmetrical distributions with similar peak magnitudes of  $M_r \approx -15$ . Lenticular galaxies show a narrower distribution than elliptical galaxies with a peak at  $M_r = -19.5$ . Among the three giant galaxies, E, S0, and Sp, spiral galaxies show the most symmetrical distribution with a peak luminosity at  $M_r = -17.5$ . Therefore, spiral galaxies are likely to be faintest among the three types of giant galaxies. It is due to the dominance of late-type spirals which becomes fainter toward the later Hubble stages (van den Bergh 1960; Strom 1980; Buta et al. 2007).

Figure 16 presents the  $u - r$  color distributions of the local galaxies which are sorted according to the broad morphological types. The color distributions depend more strongly on the morphological types than the luminosity distribution. The dependence of the color distribution on the morphological type is expected because the color of a galaxy is a widely used proxy of the galaxy morphology. As shown in Figure 16, elliptical galaxies show the narrowest color distribution centered on  $u - r \approx 2.5$ . Approximately 90% of elliptical galaxies have  $u - r$  colors between 2.2 and 3.0. The blue elliptical galaxies, which comprise  $\sim 9\%$  of all elliptical galaxies, have a blue tail. Lenticular galaxies are also likely to have red colors similar to elliptical galaxies. Approximately 73% of lenticulars have  $u - r$  colors redder than 2.2. On the other hand, spiral galaxies are likely to have blue colors. Approximately 78% of spiral galaxies have  $u - r$  colors bluer than  $u - r = 2.2$ . This makes their color distribution significantly different from that of lenticular galaxies. This shows

that the use of the colors of a galaxy as a proxy for the galaxy morphology will make a significant contamination inevitable. The color distribution of dE-like galaxies shows a double peak, one at  $u - r = 1.2$  and the other at  $u - r = 1.9$ . The blue peak is caused by the blue colors of dE<sub>blue</sub> galaxies and the red peak is due to dE and dSph galaxies. The irregular galaxies show a completely different color distribution from the others. Their peak  $u - r$  color is 1.2, which is 0.4 mag bluer than that of spiral galaxies. Only  $\sim 5\%$  of irregular galaxies are redder than  $u - r = 2.2$ .

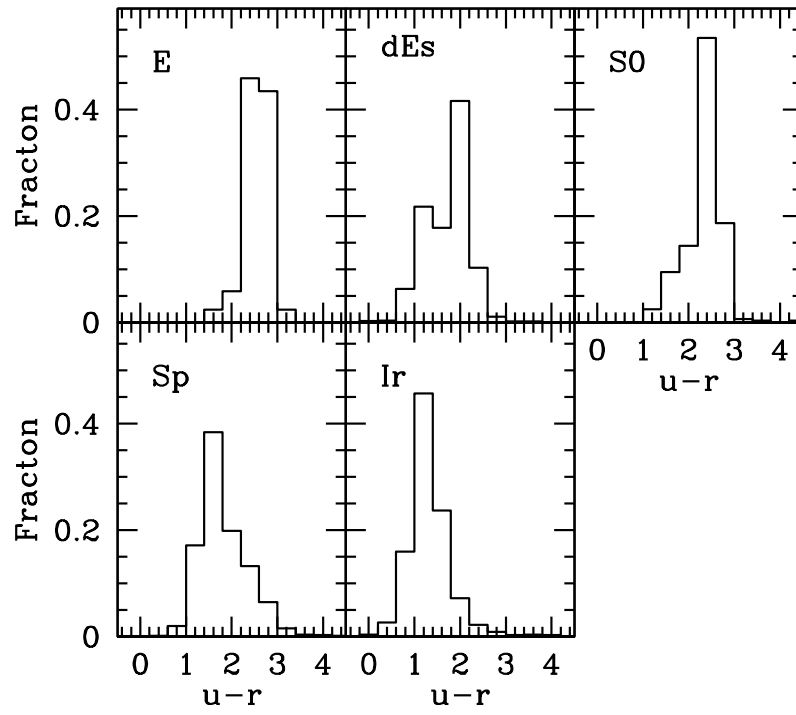


Fig. 16.— Fractional frequency distributions of  $u-r$  colors of the local galaxies.



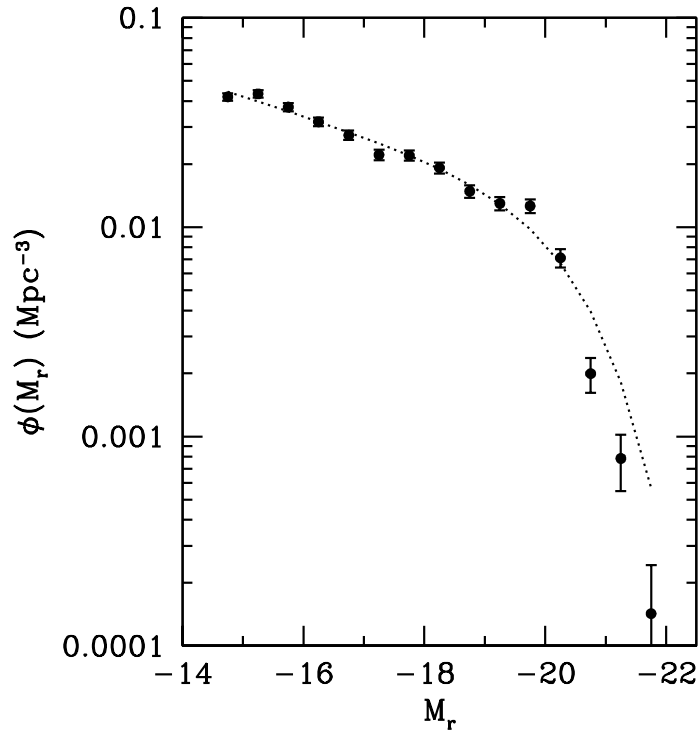


Fig. 17.— Luminosity function of the local galaxies. The best fit-Schechter function is plotted by the dotted line. Errors are Poisson errors.

Figure 17 shows the luminosity function of the local galaxies, which extends to  $M_r \approx -15$ , together with the best-fitted Schechter luminosity function (Schechter 1976) of the form

$$\phi(M)dM = 0.4 \ln 10 \phi^* [10^{-0.4(M-M^*)}]^{\alpha+1} \exp[-10^{-0.4(M-M^*)}] dM, \quad (1)$$

where  $M^*$  is the characteristic luminosity of a galaxy and  $\phi^*$  is the number density in units of  $\text{Mpc}^{-3}$ . We determined the three parameters,  $\phi^* = 0.015$ ,  $\alpha = -1.22$ , and  $M_r^* = -20.58$  by minimizing  $\chi^2$ . The drop at  $M_r > -15$  is attributed to the observation limit of the SDSS spectroscopic observation, which is set to  $r_{pet} = 17.77$ . This confines the volume-limited sample to galaxies brighter than  $M_r = -15.2$ . The rapid drop at  $M_r < -20$  is somewhat different from the luminosity functions of galaxies derived from the different volume-limited samples of different limiting magnitudes. Choi et al. (2007) derived the luminosity functions for six volume-limited samples from SDSS DR4plus. Their slopes are much shallower than the slope of the present luminosity function. The reason for the steeper gradient, i.e., the smaller  $\alpha$  in the Schechter functions, for the present sample is that the local volume is less dense than the regions outside the local universe. A similar trend for the steeper gradient in the luminosity functions of nearer samples was also observed among the volume-limited samples (Choi et al. 2007).

## 5.2. Isophotal Radius

The size of a galaxy can be defined in a variety of ways. We adopted the isophotal semi-major axis length as a representative radius of the local galaxies. Isophotal diameters can be affected by galactic extinction and inclination. We suppose that galactic extinction is negligible for the present sample due to the SDSS-covered area, however, inclination might affect the isophotal diameter. There have been a number of studies on the effect of inclination on the isophotal diameter (Holmberg 1958; de Vaucouleurs et al. 1976; Peppel et

al. 1986; Jones et al. 1996). While Holmberg (1958) assumed that the change in diameter due to the inclination of a galaxy is negligible, de Vaucouleurs et al. (1976) thought that the inclination effects are need to be corrected. However, as shown by Peppel et al. (1986) and Jones et al. (1996), it depends on the optical nature of galaxies. In the case of spiral galaxies, their disks are believed to be optically thick (Disney et al. 1989), whereas the disks of lenticular galaxies are thought to be optically thin (Michard & Simen 1993). The isophotal diameters of optically thin disks increase with inclination. The isophotal radius is calculated from the isophotal semi-major axis of the  $r$ -band image obtained from SDSS DR7. The isophotal semi-major and semi-minor axes are measured at a surface brightness ( $\mu$ ) of  $25 \text{ mag arcsec}^{-2}$  at five pass-bands ( $u, g, r, i, z$ ) in the SDSS, and are given in units of pixels. The isophotal axis lengths in the pixels are converted to kiloparsecs using a pixel size of  $0.396 \text{ arcsec}$  and the distances used to calculate the absolute magnitude. This isophotal radius is close to the Holmberg radius which is measured at  $\mu_B = 26.5 \text{ mag arcsec}^{-2}$ .

Figure 18 shows the frequency distribution of the isophotal radii of local galaxies sorted according to their broad morphological types: E, dEs, S0, Sp, and Ir. As shown in Figure 18, the distributions of the isophotal radii of galaxies depend strongly on the morphological types of the galaxies. As expected, dE-like galaxies show the narrowest distribution, which peaked at  $R_{iso} \approx 1.5 \text{ kpc}$ , and are limited to  $\sim 5 \text{ kpc}$ . The Ir class of galaxies shows a similar narrow distribution with the same peak but it extends to  $\sim 8 \text{ kpc}$ . This is because most Ir galaxies are dwarf galaxies with sizes similar to dEs. Some galaxies larger than  $R_{iso} \sim 5 \text{ kpc}$  are late-type spiral-like galaxies or peculiar galaxies, some of which are merging galaxies. The ranges of isophotal radii of the ellipticals and lenticulars are similar, even though there are large fluctuations in the ellipticals due to the small number of galaxies. Interestingly, the most probable sizes of the lenticulars and spirals are similar to each other ( $\sim 3.5 \text{ kpc}$ ) whereas the ranges of the distributions are significantly different. The sizes of the largest spirals are about two times larger than those of the lenticulars. The same is true for those

elliptical galaxies which show a similar size distribution to that of the lenticular galaxies. The reason for the double size of the spiral galaxies is thought to be the late accretion of the intergalactic material (Larson 1976; Matteucci & Francois 1989; van der Hulst & Sancisi 2004; Naab & Ostriker 2006; Combes 2014), which makes the inside-out growth of galaxies similar to that assumed for the formation of the Milky Way.

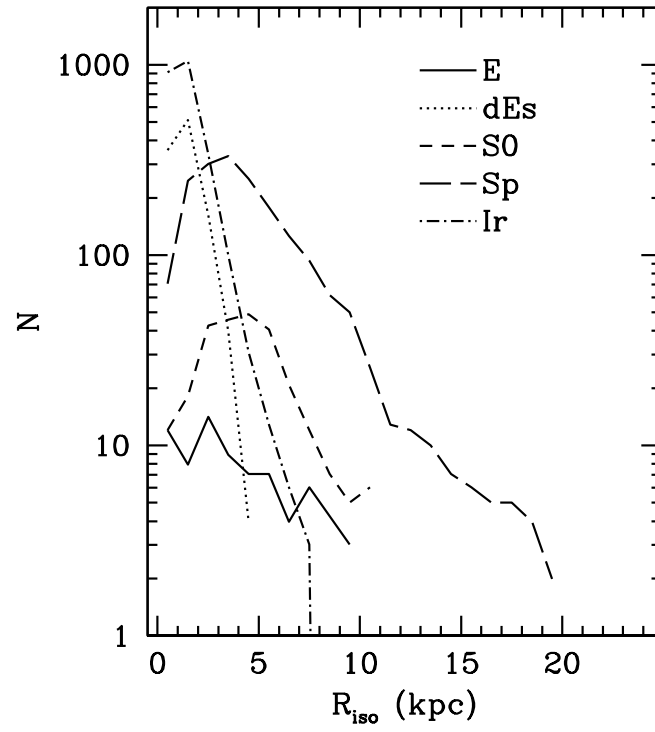


Fig. 18.— Frequency distribution of isophotal radius ( $R_{iso}$ ) of the local galaxies.

The basic properties of a galaxy such as mass, luminosity, radius, and morphology are believed to be determined by the galaxy formation process. These parameters are supposed to be correlated with each other because they have the same origin. The radius-luminosity relation (Shen et al. 2003; McIntosh et al. 2005) is an example of such a correlation. Because the galaxy size depends on the morphology, as shown in Figure 18, the interplay between the size and luminosity is supposed to be more complex. There have been many studies to investigate the morphology dependence of the radius-luminosity relation of galaxies since the pioneering work by Hubble (1926). Most of the previous studies used proxies of galaxy morphology rather than morphology itself (Strateva et al. 2001; Shen et al. 2003; McIntosh et al. 2005; Bernardi et al. 2014). For example, Shen et al. (2003) used the concentration index as a proxy of the morphology. However, as is well known from previous studies (Abraham et al. 1994, 2003; Conselice 2003; Kelly et al. 2004; Lotz et al. 2004; Park & Choi 2005; Scarlata 2007; Huertas-Company et al. 2008; Cheng et al. 2011; Cibinel et al. 2013; Willett et al. 2014), proxies are at best a crude approximation of galaxy morphological types. In this regard, Guo et al. (2009) distinguished early-type galaxies and late-type galaxies by visual inspection of the images for an analysis of the structure of central galaxies in groups and clusters. Therefore, the morphological types presented in this study will be useful to explore the interplay between the size and luminosity of galaxies. We are planning to do this in a series of forthcoming papers. We are particularly interested in the radius-luminosity relation of dwarf galaxies.

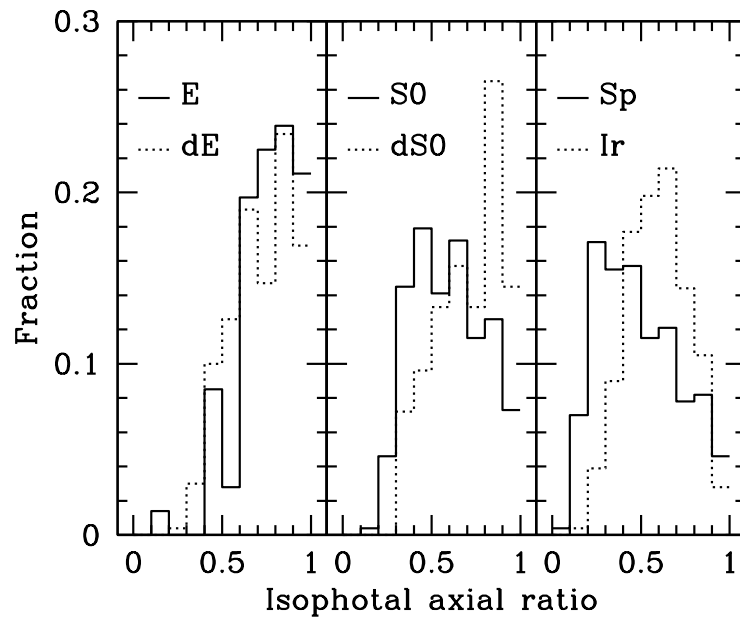


Fig. 19.— Fractional distribution of isophotal axis ratios of the local galaxies. E and dE (dwarf elliptical-like galaxies except dwarf lenticulars) are presented in the left panel, S0 and dS0 in the middle panel, and Sp and Ir in the right panel.

### 5.3. Axis Ratio

The axial ratio of a galaxy ( $b/a$ ) is closely related to the intrinsic shape of the galaxy, which is determined by its dynamical structure. Figure 19 shows the fractional frequency distributions of the axis ratios of 5836 galaxies sorted according to their morphological types. The isophotal semi-major and semi-minor axes in  $r$ -band, which are measured at a surface brightness of  $25 \text{ mag arcsec}^{-2}$ , are used. Figure 19 plots the three morphological types of giant galaxies (E, S0, and Sp) compared to their dwarf cousins (dE and dS0) for E and S0 galaxies and irregular galaxies for spiral galaxies. The axis ratio distributions of the ellipticals and dE (left panel) are similar, whereas a significant difference was observed in the lenticular and dwarf lenticular galaxies (middle panel) as well as in spiral galaxies (right panel). The solid lines represent the giant galaxies and the dotted lines indicate the dwarf counterparts.

Although the general shapes of the axis ratio distributions of the giant elliptical galaxies and dE galaxies are similar, there are some differences between the two. Dwarf elliptical galaxies have a higher fraction of galaxies with  $b/a < 0.5$  than giant elliptical galaxies, even though the smallest  $b/a$  is observed in a giant elliptical galaxy. On the other hand, the morphological type of this galaxy (NGC 2768) is controversial. It is classified as E6 in RC3, whereas the morphological type adopted by the NED is S0, which was taken from The Carnegie Atlas of Galaxies (Sandage & Bedke 1994). The more flattened structure of dE galaxies is consistent with those observations showing fast rotation in a considerable fraction of dE galaxies (Geha et al. 2010). On the contrary, the general similarity of the axis ratio distributions of the giant and dwarf elliptical galaxies suggests that a large fraction of dwarf elliptical galaxies are dispersion-supported systems like giant elliptical galaxies.

The dissimilarity of the axis ratio distributions of giant and dwarf lenticular galaxies is quite interesting because dS0s are considered to be low-luminosity versions of S0s (Aguerri



et al. 2005). The axis ratio distribution for dS0s in Figure 19 seems to show well that the dS0s should not be thought of as small versions of S0s. Rather, they are close to dE galaxies because their axis ratio distribution is similar to that of dE galaxies. The lack of dS0s with an isophotal axis ratio ( $b/a$ ) less than 0.3 suggests that they are intrinsically thicker than S0s. The lack of small axis ratios is also observed in dE and irregulars, suggesting less flattened shapes for these galaxies. The thick intrinsic shape of irregular galaxies is consistent with earlier studies (Heidmann et al. 1972; van den Bergh 1988; Roychowdhury et al. 2010).

The dissimilar distributions of the axis ratios of spiral galaxies and irregular galaxies shown in the right panel of Figure 19 are believed to be caused by the real difference in their dynamical structures because the statistical noises are small enough to be ignored due to the large number of spiral and irregular galaxies. In the case of lenticular galaxies, the axis ratio distribution of which is supposed to be similar to that of the spiral galaxies. We can see a large fluctuation in the histogram due to the small number of lenticular galaxies, which is about one-seventh that of the spiral galaxies. The larger fraction of small axis ratios in spiral galaxies is due to the rotating disks of spiral galaxies, the orientations of which are random, whereas the lack of small axis ratios in the irregular galaxies is believed to be due to the triaxial nature of irregular galaxies (van den Bergh 1988).

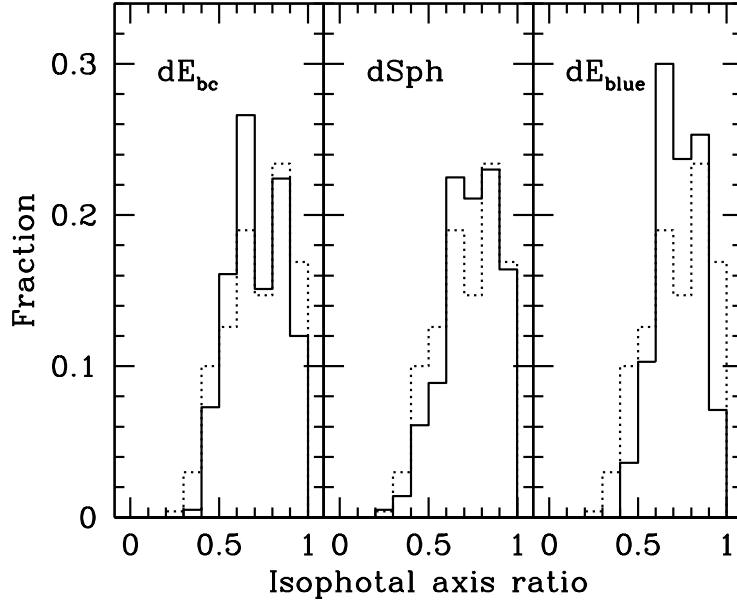


Fig. 20.— Fractional distribution of isophotal axis ratios of the local galaxies. Blue-cored dwarf ellipticals (dE<sub>bc</sub>) in the left panel, dwarf spheroidals (dSph) in the middle panel, and blue dwarf ellipticals (dE<sub>blue</sub>) in the right panel. Histograms plotted by the dotted lines are those for the dwarf ellipticals (dE).

Figure 20 shows the fractional distribution of the axis ratios of the dwarf elliptical-like galaxies; dE<sub>bc</sub> galaxies in the left panel, dSph galaxies in the middle panel, and dE<sub>blue</sub> galaxies in the right panel. The axis ratio distribution of dE galaxies (dotted lines) is also plotted for comparison. Due to the small numbers, there are large fluctuations in the histograms but there seem to be some differences among the subtypes of dE-like galaxies. The most pronounced difference is observed between dE and dE<sub>blue</sub> galaxies. It is due to the narrow range of axis ratio distribution of dE<sub>blue</sub> galaxies with a lower limit of  $b/a = 0.4$ . Approximately 80% of dE<sub>blue</sub> galaxies have axis ratios between  $b/a = 0.6$  and  $b/a = 0.9$ . This suggests that they are mostly dispersion-supported systems but are not as round as dSph galaxies and dispersion-supported dE galaxies. The lack of a systematic difference between dE and dE<sub>bc</sub> is consistent with the morphological similarity between the two types of galaxies, except for the presence of blue cores in dE<sub>bc</sub> galaxies. The axis ratio distribution of dSph galaxies is similar to that of dE galaxies but the lower fraction of galaxies with small  $b/a$  appears to be real because they are systematically lower than that of dE galaxies for a small axis ratio ( $b/a \lesssim 0.4$ ). The lack of galaxies with a small  $b/a$  is consistent with the kinematic observations of dSph galaxies (Salucci et al. 2012).

## 5.4. Morphological Properties of Dwarf galaxies

### 5.4.1. Dwarf Ellipticals and Blue-cored Dwarf Ellipticals

The morphology of dwarf elliptical galaxies is characterized by their round appearance and red colors, similar to that of giant elliptical galaxies. On the other hand, there are some differences in the photometric properties between dE and giant ellipticals. For example, dE galaxies exhibit lower surface brightness and a shallower luminosity gradient than giant elliptical galaxies. The mean luminosity of dE galaxies is  $M_r = -15.9 \pm 1.0$ , which is approximately 3.5 mag fainter than the mean luminosity ( $M_r \approx -19.5$ ) of elliptical galaxies

listed in the present catalog. Wirth & Gallagher (1984), Kormendy (1985), and Kormendy et al. (2009) argued that these differences result from the structural difference between dE and giant ellipticals. Therefore, dE galaxies cannot simply be a small version of giant elliptical galaxies (Kormendy & Bender (2012, and references therein). The real dwarf counterparts of giant elliptical galaxies are compact elliptical galaxies, exemplified by M32 (Ferguson & Binggeli 1994; Kormendy et al. 2009). They have sizes comparable to dwarf elliptical galaxies but have a high surface brightness. On the other hand, Jerjen & Binggeli (1997) and Graham & Guzman (2003) argued that the scaling relations of the dwarf elliptical galaxies are continuations of those of giant elliptical galaxies because the nonlinear relations between the absolute magnitude and the effective surface brightness or effective radius are consequences of the two linear relations between the stellar concentration, quantified by the Sersic index  $n$ , and stellar mass or central surface brightness. Their structural characteristics are not distinguished from those of giant elliptical galaxies (Graham 2013, and references therein). Whether or not dE galaxies are distinct populations, they are thought to be a mixture of kinematically heterogeneous populations (Geha et al. 2010), the origins of which are thought to be different (Lisker 2009; Toloba et al. 2012; Lisker et al. 2013).

The three subtypes of dE-like galaxies,  $\text{dE}_{un}$ ,  $\text{dE}_n$  and  $\text{dE}_{bc}$ , have similar structure except for the nuclear morphology. Normally, the blue cores of  $\text{dE}_{bc}$  galaxies are larger than the star-like nuclei in  $\text{dE}_n$  galaxies but in some cases, they appear small. However, we classify them as  $\text{dE}_{bc}$  galaxy if their colors are blue enough to assume the presence of young stellar populations. The number of  $\text{dE}_{bc}$  galaxies that have a small core is negligibly small. The global colors of  $\text{dE}_{bc}$  galaxies are similar to those of  $\text{dE}_{un}$  and  $\text{dE}_n$  galaxies. However, in some cases, their colors appear quite blue close to  $\text{dE}_{blue}$  galaxies.

The well-known examples of  $\text{dE}_{bc}$  galaxies are NGC 185 (Hodge 1963) and NGC 205

(Hodge 1973), both of which are satellite galaxies of M 31. The blue cores of dE<sub>bc</sub> galaxies are thought to be due to recent star formation. Different scenarios have been proposed for the origin of the gas in the center of dE<sub>bc</sub> galaxies. The gas left in the spiral and irregular galaxies which are transformed into dE by ram pressure stripping (Gunn & Gott 1972) or galaxy harassment (Moore et al. 1996, 1998) is widely considered for the origin of the central star formation of dE<sub>bc</sub> galaxies in cluster environment (Lisker et al. 2006, 2007; Pak et al. 2014). On the other hand, gas accretion from the cosmic web (Hallenbeck et al. 2012) can be responsible for the isolated dE<sub>bc</sub> galaxies such as IC 125 (Gu et al. 2006). In addition, it is possible that small cores such as star-like blue nuclei are made from recycled gas from evolved stars (Boselli 2008; Hallenbeck et al. 2012).

#### 5.4.2. Dwarf Spheroidals

The morphology of dSph galaxies is similar to that of dwarf elliptical galaxies. They share a round appearance and red color, lower surface brightness, and shallower gradient in the surface brightness than elliptical galaxies. This is why many studies did not distinguish them (Kormendy & Bender 2012). On the other hand, there are some differences in their morphological properties. On average, they are fainter than dE galaxies. They have a mean luminosity of  $M_r = -14.4 \pm 1.2$ , which is  $\sim 1.5$  mag fainter than the dE galaxies. In addition, they differ in their surface brightness distribution. The surface brightness of dSph galaxies is, on average, fainter than that of dE galaxies. Also, dSph galaxies show a gentler gradient in their surface brightness distribution than dE galaxies. The low luminosity and low surface brightness of dSph galaxies are consistent with the relation between the luminosity and surface brightness of a galaxy (Sandage & Binggeli 1984).

In addition to the difference in surface brightness between dSph galaxies and dE galaxies, there are some properties that are quite different. The presence of a blue core is

barely observed in the dSph galaxies, whereas a significant fraction of dE galaxies have blue cores. Some difference in the axis ratio distributions is present, showing smaller fractions of highly flattened dSph galaxies. Because axis ratios, i.e., ellipticities are closely related to the degree of rotational support (Binney 1978), dSph galaxies are believed to be mostly a dispersion-supported system, whereas dE galaxies are considered to be partially supported by rotation. This picture of kinematic properties of dSph galaxies is frequently addressed in previous observations (Walker et al. 2009; Toloba et al. 2012). On the other hand, the distinction of ellipticity distributions between dSph and dE is not as clear as that in the fast and slow rotating elliptical galaxies observed in the ATLAS (Weijmans et al. 2014) due to the fact that the fractions of rotationally supported dEs and dispersion-supported dEs are similar (Geha et al. 2010). However, the differences in photometry as well as in kinematics between the dSph and dE galaxies suggest that they have different origins. It is quite likely that dSph galaxies are primordial objects formed at  $z > 7$  (Kormendy 2014), while dE galaxies, at least fast rotating dE galaxies, are stripped late type galaxies.

#### 5.4.3. *Blue Dwarf Ellipticals*

The morphological distinction of dE<sub>blue</sub> galaxies from other dwarf galaxies is one of the most successful uses of color images in morphology classification. While the blue colors of blue elliptical galaxies (Strateva et al. 2001), which distinguish them from normal elliptical galaxies, are believed to be due to recent star formation in the core regions, the colors of the dE<sub>blue</sub> galaxies are due to global star formation that makes their colors much bluer than the dwarf elliptical galaxies. These galaxies have similar colors to those of irregular galaxies. Their shapes, however, are quite similar to those of dE galaxies although their axis ratio distribution is somewhat different. dE<sub>bc</sub> are considered to be much different from the dE<sub>blue</sub> galaxies because dE<sub>bc</sub> galaxies have red colors outside the blue core. In some aspects, the

$\text{dE}_{\text{blue}}$  galaxies are similar to HII region-like BCDs or dI. The former shows somewhat bluer colors than  $\text{dE}_{\text{blue}}$  but with a similar shape, and the latter shows a lack of axial symmetry compared to  $\text{dE}_{\text{blue}}$ .

#### 5.4.4. *Dwarf Lenticulars*

The morphology of dwarf lenticular galaxies (dS0) is similar to their giant cousin, lenticular galaxies (S0), in the sense that they show subtle structure, such as the bulge and disks in S0s. On the other hand, they are significantly different from S0s in many aspects. The morphology of the central excess of light in dwarf lenticular galaxies appears to be lens-like (Sandage & Binggeli 1984) and much less massive than a bulge. In some cases, the lens component is quite large in size but their luminosity seems to be low. They are likely to have star-like nuclei, which causes them to be classified as  $\text{dS0}_n$ , similar to the nucleated dwarf elliptical galaxies,  $\text{dE}_n$ . Their colors are also similar to dwarf ellipticals. In addition, it is quite rare to have bars inside and there appears to be no inner and outer rings in the dwarf lenticular galaxies. The absence of inner and outer rings in dwarf lenticular galaxies is expected if they are stripped, former late-type galaxies. Rings are a phenomenon mainly of massive early-type galaxies. They are virtually never seen among extreme late-type spirals or magellanic irregulars (Buta & Combes 1996; Buta et al. 1998). On the other hand, they are likely to show disrupted features in the outer parts of the galaxies. These features are probably remnants of spiral arms. If this is the case, dwarf spirals can be formed in disks as small as those of dwarf lenticular galaxies but can not survive long due to the lack of sufficient mass to protect them from tidal or hydrodynamic disturbances.

#### 5.4.5. *Blue Compact Dwarfs*

Compact galaxies are distinguished from others by their high surface brightnesses which are brighter than  $20 \text{ mag arcsec}^{-2}$  (Zwicky & Zwicky 1971). A BCD galaxy has very blue color indicative of a likely starburst. BCDs show a range of morphologies in the present catalog. One extreme case is a BCD whose morphology is characterized by a HII region-like appearance, and the other extreme case is characterized by localized compact regions of intense bursts of star formation within a larger irregular galaxy. Examples of the two extreme cases are presented in the two rightmost columns of the bottom row in Figure 5.

The HII region-like BCDs similar to those observed by Thuan & Martin (1981) who chose their samples mostly from the earlier objective prism surveys. The shape of these galaxies is similar to the small-sized  $\text{dE}_{\text{blue}}$  galaxies but they have deep bluer colors. Because there is no clear color distinction between these two types of galaxies, they can be classified as genuine BCDs or isolated extragalactic HII regions (Sargent & Searle 1970). On the other hand, the selection of small-sized  $\text{dE}_{\text{blue}}$  galaxies from the  $\text{dE}_{\text{blue}}$  sample of galaxies is also subjective. The other types of BCDs are basically irregular galaxies with localized compact regions of intense star-bursts. The size of the compact regions of extreme star-burst varies from the size of HII regions to the galaxy size. Therefore, it is also subjective to set a size-limit when selecting BCDs. In the present study, a galaxy is classified as BCD if the size of the compact regions of extreme star burst is larger than  $\sim 20\%$  of the galaxy size. In order to distinguish the irregular galaxies with small star burst regions, we assign Im/BCD as the morphological type of these galaxies. They are amount to  $\sim 20\%$  of irregular galaxies.



#### 5.4.6. *Dwarf Irregulars*

The majority of galaxies in the local universe are dwarf galaxies if we consider irregular galaxies fainter than  $M_r \approx -17$  to be dwarf galaxies, even though we classify them as Im galaxies because of morphologies resembling the late-type spirals. dI galaxies show a range of morphologies from very simple shapes to a high degree of complexity. dI with a simple morphology resemble  $dE_{blue}$  or BCDs. The only difference is the degree of roundness. dI galaxies with complex morphologies are caused mainly by sites of intense star formation. They are too small to drive the global density waves. Star formation in dI galaxies is believed to be caused by self-propagating star formation (Gerola & Seiden 1978). Interactions with neighboring galaxies makes their morphology rounder and rounder if the interactions occur frequently. The morphology of some dI galaxies show a transition type from dI to dE/dSph or vice versa.

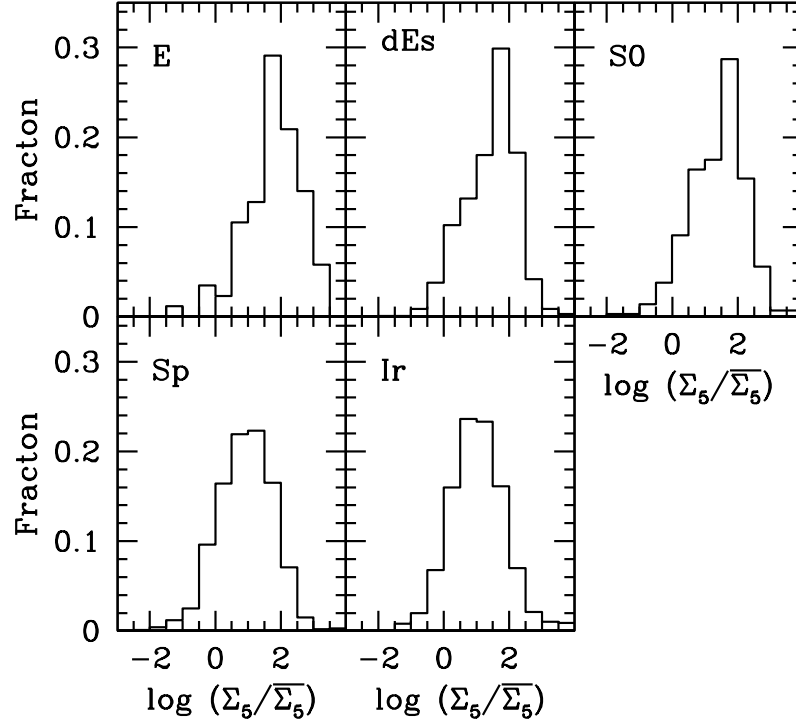


Fig. 21.— Fractional distributions of the local background density  $\Sigma_5$  normalized by the mean local background density  $\bar{\Sigma}_5$ .

## 6. Environment Dependence of Morphology

### 6.1. Local Background Density

The morphology of a galaxy is dependent on its environment. This dependence has been represented by the morphology-density relation since the pioneering work of Dressler (1980). There are a variety of ways to measure the local background density of a galaxy (Muldrew 2012). Recently, Ann (2014) explored the dependence of disk morphology on the local background density derived from the  $n$ th nearest neighbor method with  $n = 5$ ,  $\Sigma_5$ , which is defined as

$$\Sigma_5 = \frac{5}{4\pi r_{p,5}^2}, \quad (2)$$

where  $r_{p,5}$  is the projected distance to the fifth nearest galaxy brighter than  $M_r = -15.2$  with  $|\Delta V| < 1000 \text{ km s}^{-1}$ . We normalized  $\Sigma_5$  by the mean local background density ( $\bar{\Sigma}_5$ ).

Figure 21 shows the fractional density distribution of local galaxies sorted by the broad morphological types. As shown in Figure 21, the distributions of the local background density of galaxies with different morphology differ greatly. Elliptical galaxies are most frequent in the high-density regions, forming a narrow peak at the high-density regions with an extended tail toward the low-density regions, whereas spiral and irregular galaxies show approximately symmetrical distributions with a peak density at  $\log(\Sigma_5/\bar{\Sigma}_5) = 0.75$ . Lenticular and dE-like galaxies show similar density distributions to that of elliptical galaxies with a slightly larger fraction of galaxies in the low-density regions than elliptical galaxies. It is worth noting that dE-like galaxies do not obey the luminosity-density relation (Park et al. 2007) because it dictates that dwarf galaxies which are basically much less luminous than elliptical and lenticular galaxies are located preferentially in the low-density regions. This means that the morphology of a galaxy, particularly a dwarf galaxy, can be affected greatly by other environmental properties. The interactions with large galaxies to which most of dwarf galaxies are bound as satellite galaxies are considered to be the main

cause of the secondary parameter affecting the dwarf galaxy morphology. The distance to the nearest neighbor ( $r_p$ ) appears to be a good measure of the galaxy environment because the effect of interactions depends on the separation between the interacting galaxies.

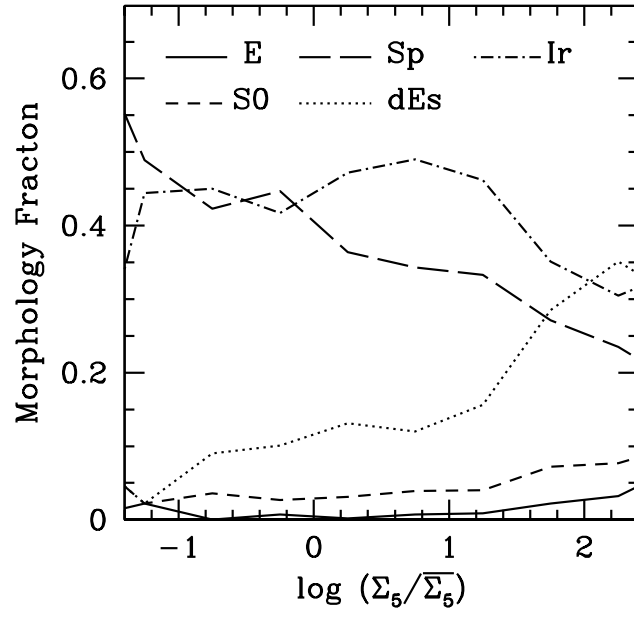


Fig. 22.— Morphology fraction as a function of the local background density.

To see the dependence of the galaxy morphology on the local background density, the fraction of galaxy morphological types is plotted as a function of the local background density (Figure 22). In general, they follow the morphology-density relation, i.e., the fractions of early type galaxies (E, S0, and dEs) increase with increasing local background density, whereas those of late type galaxies (Sp and Ir) decrease with increasing density. Although the general pattern of increasing fractions with increasing local background density is the same for the three classes of early type galaxies, there are some differences between them. Fractions of the two early type giant galaxies (E and S0) show an almost flat distributions at  $\log (\Sigma_5/\bar{\Sigma}_5) < 1$  and gradual increase thereafter, whereas that of the early type dwarf galaxies (dEs) shows a nearly monotonic increase with increasing density with a sudden change of the slope at  $\log (\Sigma_5/\bar{\Sigma}_5) \approx 0.8$ . Irregular galaxies show a nearly opposite trend from that of dEs at  $\log (\Sigma_5/\bar{\Sigma}_5) \gtrsim 0.8$  and a somewhat flat distribution at  $\log (\Sigma_5/\bar{\Sigma}_5) \lesssim 0.8$  with a local minimum around  $\log (\Sigma_5/\bar{\Sigma}_5) \approx -0.8$ . On the other hand, spiral galaxies demonstrate behavior opposite of the general trend for early-type galaxies, that is, an almost monotonically decreasing spiral fraction with increasing local background density. Also, there is not much variation in the fractions of Hubble stages and bar types of spiral galaxies along the local background density except for an increasing early spiral fraction and a decreasing late spiral fraction with increasing local background density in high-density regions,  $\log (\Sigma_5/\bar{\Sigma}_5) > 1$ .

To observe the dwarf morphology dependence on the local background density, we plot the distribution of the morphology fractions of dwarf galaxies as a function of the local background density in Figure 23. A clear difference in the morphology distribution can be seen between the two groups of dwarf galaxies. One group of dwarf galaxies (dE, dSph, and dS0) shows similar fractions with an increasing trend for the density ranges of  $\log (\Sigma_5/\bar{\Sigma}_5) < 1.2$  and become different fractions at the higher density regions. The other group (dE<sub>bc</sub> and dE<sub>blue</sub>) shows dominant fractions at local background densities less than

the mean local background density. They comprise more than 90% of the dEs galaxies at  $\log (\Sigma_5/\bar{\Sigma}_5) < 0$ , and decrease with increasing density to become the same fractions as those of the former group at  $\log (\Sigma_5/\bar{\Sigma}_5) \approx 1.3$ . The predominance of dE<sub>blue</sub> galaxies in the low-density regions seems to reflect the environmental dependence of the star formation rate observed in the local universe, and higher star formation rate in the low-density regions (Lewis et al. 2002; Gomez et al. 2003; Tanaka et al. 2004), in accord with down-sizing (Cowie 1996). The high fraction of star forming dwarfs in the low-density regions is due to the dependence of collapse time ( $\tau$ ) of the pre-galactic cloud on the background density ( $\tau \propto \rho^{-1/2}$ ). In the low-density regions, a large amount of gas is left to make dwarf galaxies in the present epoch, including dE<sub>blue</sub> galaxies. The preference for dE<sub>bc</sub> galaxies in low-density regions can be understood if late gas accretion is the main cause of the central star formation in the isolated dE<sub>bc</sub> galaxies.

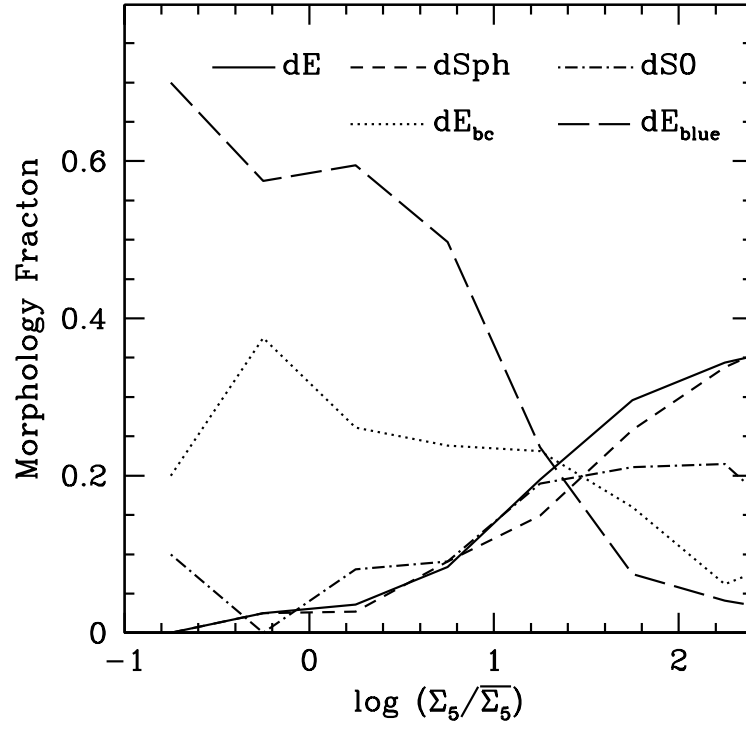


Fig. 23.— Morphology fraction of dwarf elliptical-like galaxies as a function of the local background density.



Although the local background density appears to be the primary parameter dictating the morphology of a galaxy, its role is different for giant galaxies and dwarf galaxies. For giant galaxies, it constrains the galaxy morphology through the star formation efficiency, which depends on the dynamical timescales ( $\tau \propto \rho^{-1/2}$ ) at the initial collapse phase and the subsequent hierarchical merging phase of galaxy formation. In contrast, for dwarf galaxies, it constrains the interaction rates with giant galaxies. In cases of dwarf galaxies that are bound to giant galaxies as satellites, the interaction rate is inversely proportional to the orbital period that is determined by the dynamical timescales. Therefore, dE, dSph, and dwarf lenticulars, which are likely to be located in the high-density regions, are supposed to lose their gas quickly due to the frequent interactions with large galaxies. On the other hand, dE<sub>blue</sub> galaxies have fewer interactions than other dE-like galaxies to retain their gas longer. In the case of the dE<sub>bc</sub>, the role of local background density seems to be complicated. Since dE<sub>bc</sub> are similar to dE galaxies except for the blue core, their red color outside the nucleus suggests early removal of gas by frequent interactions with giant galaxies, but there is leftover gas in their environment to accrete the gas removed from dEs to make blue core.

## 6.2. Nearest Neighbor

The morphologies of galaxies are affected by the neighboring galaxies. One of the measures of the influence of the neighbor galaxies is the projected distance,  $r_p$ . This can be expressed in absolute units such as Mpc, but  $r_{p,n}$ , which is normalized by the neighbor’s virial radius, is a good measure of the local environment because the morphology of a galaxy is affected significantly by the neighbor galaxy when it is located within the neighbor’s virial radius (Park et al. 2008; Park & Choi 2009). The virial radius of a galaxy is defined as the radius where the mean density inside the radius becomes the virialized density, which is set to  $766 \bar{\rho}$  (Park et al. 2007). The virial radius of a galaxy was calculated according

to that described in Park et al. (2007). We derived  $r_p$  of the 5836 local galaxies using the same neighbor search conditions as those applied to derive the local background density.

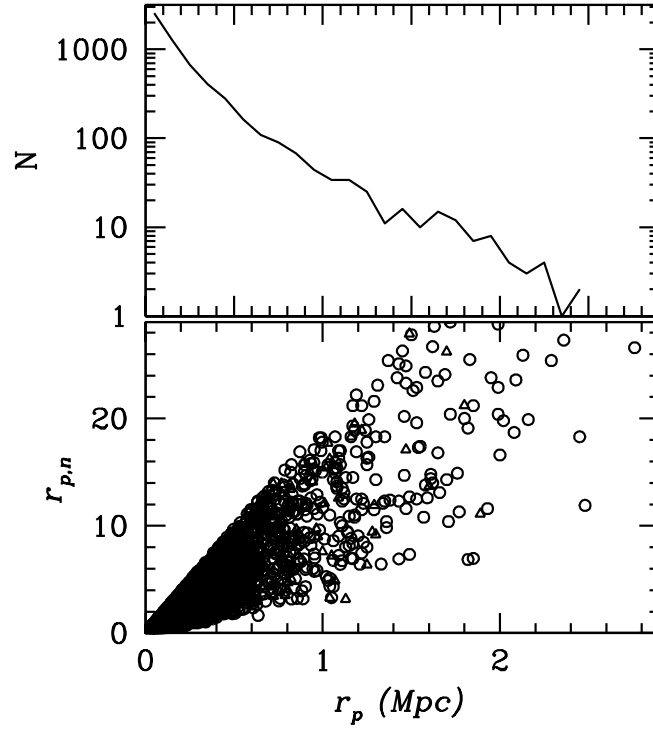


Fig. 24.— Projected distance to the nearest neighbor galaxy  $r_p$ . The frequency distribution of  $r_p$  (Mpc) is plotted in the upper panel and the scatter diagram of  $r_{p,n}$  and  $r_p$  (Mpc) is presented in the lower panel.

Figure 24 shows the frequency distribution of  $r_p$  (Mpc; upper panel) and the scatter diagram of  $r_{p,n}$  and  $r_p$  (Mpc). The frequency distribution in the upper panel shows a very rapid decrease of number of galaxies with increasing  $r_p$ . Approximately 40% of the local galaxies have a neighbor galaxy within  $r_p = 0.1\text{Mpc}$  and similar fractions of the local galaxies are located inside the virial radius of the nearest neighbor. Owing to the rapid decrease of the frequency distribution of  $r_p$ , the number of galaxies that have their nearest neighbors at  $r_p > 1\text{Mpc}$  is only 204 (3.5%) and it is reduced to 66 ( $\sim 1\%$ ) for  $r_p > 2\text{Mpc}$ . A good correlation is observed between  $r_{p,n}$  and  $r_p$  (Mpc) with an upper envelope of an almost straight line. The scatter is caused by the wide range of virial radii of galaxies. The upper envelope is due to the smallest dwarf galaxies while the lower envelope is due to the largest giant galaxies. Because of the small number of large giant galaxies, the lower envelope is not so straight as the upper envelope.

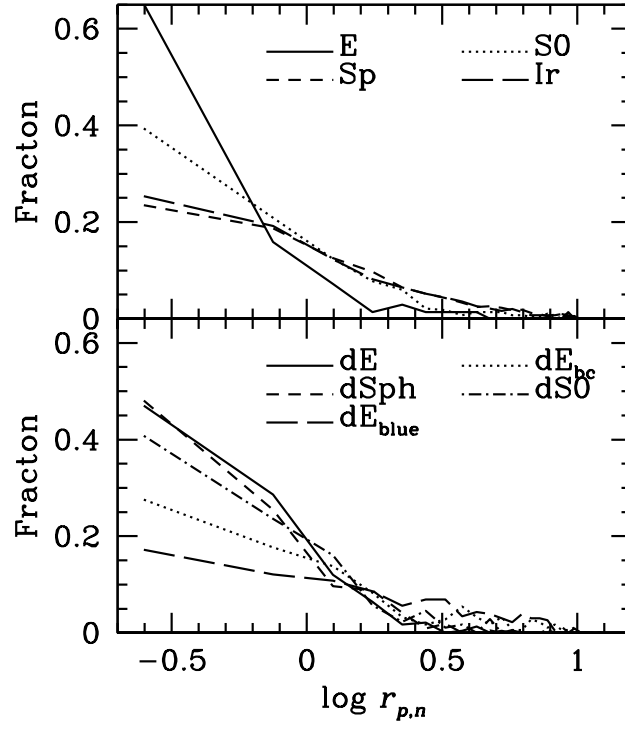


Fig. 25.— Fractional distributions of morphological types as a function of  $r_{p,n}$ , four broad types of E, S0, Sp, and Ir in the upper panel, and dEs in the lower panel.

Figure 25 shows the fractional distributions of the morphological types as a function of  $r_{p,n}$ . It is apparent that the majority of local galaxies are located within the virial radius of the nearest neighbor. Among the morphological types of giant galaxies, the elliptical galaxies are most likely located within the virial radius of the nearest neighbor, whereas more than half of the spiral and irregular galaxies are located outside the neighbor’s virial radius. This means that the effects of hydrodynamical interactions with neighboring galaxies are more important in elliptical galaxies because hydrodynamical interactions are likely to be effective when a galaxy is located within the neighbor’s virial radius. Lenticular galaxies show an intermediate distribution between elliptical galaxies and spiral galaxies. Among the dE-like galaxies, dE, dSph, and dS0 galaxies show fractional distributions similar to that of lenticular galaxies, whereas dE<sub>blue</sub> galaxies show a more extended tail toward large  $r_{p,n}$ . More than  $\sim 40\%$  of dE, dSph, and dS0 galaxies are located at  $r_{p,n} > 0.5$ . The dE<sub>bc</sub> galaxies show intermediate distribution between dE and dE<sub>blue</sub>. An examination of the morphology fractions of the 5 broad morphological types as a function of  $r_{p,n}$  shows similar trends to those observed in Figure 22 where the morphological fractions are plotted as a function of the local background density. That is, the three early types (E, S0, and dEs) show increasing fractions with decreasing  $r_{p,n}$  and the two late types (Sp and Ir) show the opposite trend.

Figure 26 shows the early type fractions of the target galaxies as a function of  $r_{p,n}$ . The early-type fractions of the target galaxies increase with decreasing  $r_{p,n}$ . However, the increasing rates depend on the neighbor’s morphology. Here, early type represents three broad types of galaxy, E, S0, and dEs, whereas late type represents spiral and irregular galaxies. The early type fractions increase rapidly with decreasing  $r_{p,n}$  when the neighbor galaxy is the early-type galaxy. Whereas early-type fractions increase slowly with decreasing  $r_{p,n}$  when the neighbor galaxy is a late type. This makes the early-type fraction of the target galaxies with the early-type neighbor larger than 0.5 when they are located in the neighbor’s virial radius, whereas that of the target galaxies with the late type neighbor becomes  $\sim 0.3$ . This phenomenon was interpreted as morphological conformity between close neighbors (Park et al. 2008). The gradual increase in the early-type fraction of the target galaxies with late-type neighbor when they come closer to the neighbor suggests that the effect of the tidal interactions dominates other interactions such as hydrodynamical interactions for gas transfer from the late-type neighbor to the target galaxy. In the case of early-type neighbors, hydrodynamical interactions enhance the effect of tidal interactions by removing gas to produce a rapid increase in the early type fraction when they become closer to the neighbor.

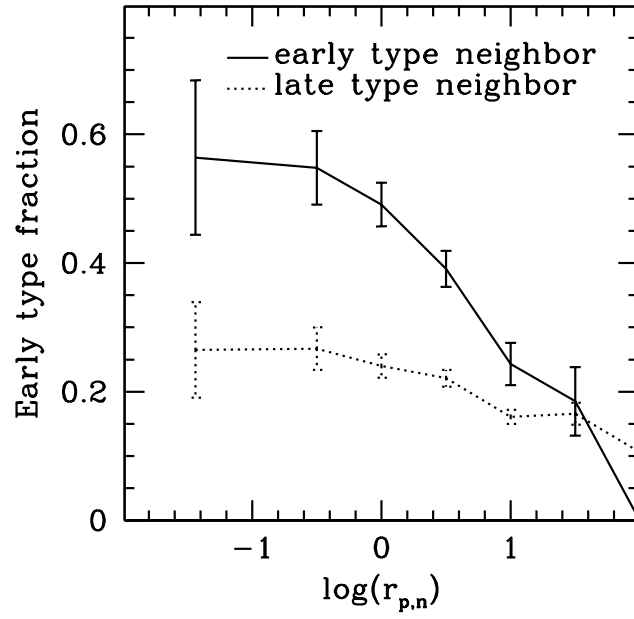


Fig. 26.— Early-type fractions as a function of  $r_{p,n}$ .



## 7. Summary and Discussion

This paper presents a catalog of the morphological types of 5836 galaxies whose redshifts are less than  $z = 0.01$ . The morphological types are determined by a visual inspection of the color images provided by SDSS DR7. The majority of galaxies in the present sample come from the KIAS-VAGC which is based on the spectroscopic target galaxies of the SDSS DR7 complemented by the bright galaxies with known redshifts from various catalogs. Galaxies fainter than the limiting magnitude of the SDSS spectroscopic target galaxies were also included if redshifts are available in the NED. The number of galaxies fainter than  $r_{pet} = 17.77$  is 809 which is approximately 14% of the present sample. Therefore, the present sample is not flux-limited but a flux-limited sample can be defined if galaxies brighter than  $r_{pet} = 17.77$  are used because galaxies brighter than the SDSS bright limiting magnitude of  $r_{pet} = 14.5$  are believed to be compiled almost completely in the NED.

The galaxy morphology classification system adopted for bright galaxies in the present study is basically the de Vaucouleurs revised Hubble-Sandage system of stages and families (Hubble 1936; de Vaucouleurs 1959; Sandage 1961; Buta et al. 2007). Inner and outer ring varieties, lenses and stages of E and S0 galaxies are not recognized in our catalog. For dwarf galaxies, we use notation similar to Binggeli et al. (1985), modified to allow for features, such as blue cores or blue colors, that are recognizable in color images. That is, we distinguish subtypes; dE, dE<sub>bc</sub>, dSph, dE<sub>blue</sub>, and dwarf lenticulars (dS0). The dE, dSph and dS0 galaxies are further divided into dE<sub>un</sub>, dE<sub>n</sub>, dSph<sub>un</sub>, dSph<sub>n</sub>, dS0<sub>un</sub>, and dS0<sub>n</sub> to denote the presence of nucleation. In the analysis of the frequency distributions, however, we do not distinguish them because physical properties, such as the color and luminosity are similar, and the numbers of dE<sub>un</sub> and dSph<sub>un</sub> galaxies are much smaller than those of dE<sub>n</sub> and dSph<sub>n</sub> galaxies.

The present catalog contains 85 elliptical galaxies (E: 1.5%), 1093 dwarf elliptical-like galaxies (dEs: 18.7%), 286 lenticular galaxies (S0: 4.9%), 1874 spiral galaxies (Sp: 32.1%), and 2498 irregular galaxies (Ir: 42.8%). Since most irregular galaxies are dwarf galaxies, the local universe is dominated by dwarf galaxies. Among giant galaxies, spiral galaxies dominate the local universe. The late-type spirals are more frequent than the early-type spirals and  $\sim 62\%$  of spiral galaxies have bars including weak bars. A significant number of dE<sub>blue</sub> galaxies, which are generally smaller than the ordinary dE galaxies, are included in the present catalog. Some dE<sub>blue</sub> galaxies have large cores that are somewhat bluer than the global colors. Most dE<sub>blue</sub> galaxies without cores are quite compact, similar to HII region-like BCDs. The only difference between these two types is the degree of star formation. HII region-like BCDs are bluer than dE<sub>blue</sub> galaxies. A considerable number of dI galaxies show somewhat round shapes with size, luminosity, and color similar to dE<sub>blue</sub> galaxies. Their environments, represented by the local background density, are also similar. Therefore, we suppose that dE<sub>blue</sub> galaxies are the same populations as dI galaxies both of which served as the building blocks of giant galaxies.

Some evidence exists for dichotomy in the morphological properties of dE galaxies and dSph galaxies, which is in contrast to the conventional practice to treat them as the same class of galaxies (Kormendy & Bender 2012). The dichotomy is not as clear as that between the giant elliptical galaxies and the dE galaxies in terms of size and luminosity. However, they are different in the surface brightness and color. The colors of the dE galaxies are similar to those of giant elliptical galaxies, whereas they differ appreciably from dSph galaxies. The surface brightness and surface brightness gradient of dwarf elliptical galaxies are intermediate between the giant elliptical galaxies and dwarf spheroidal galaxies. If we consider the kinematic difference between dSph and dE galaxies (Walker et al. 2009; Geha et al. 2010; Toloba et al. 2012), the origins of dSph and dE galaxies thought to be different, at least for the dispersion-supported dS0 galaxies and the fast rotating dE galaxies,

Dispersion-supported dSph galaxies can be promordial objects (Kormendy 2014) while fast rotating dE galaxies are stripped late type spirals (Kormendy & Bender 2012).

We explored the physical properties, such as luminosity, color, size, and axial ratios, of the local galaxies. In general, distributions of the physical parameters of galaxies with different morphological types are quite different in terms of the most probable values and the shapes of their distributions. Elliptical galaxies show the highest luminosity but their maximum size is smaller than that of spiral galaxies. The larger size of spiral galaxies is supposed to be due to the accretion of the intergalactic material after the collapse phase of galaxy formation. The luminosity and size distributions of the two types of dwarf galaxies, dEs and dIrr, are very similar, implying similar masses. The dependence of galaxy size and luminosity on galaxy morphology seems to have originated from the morphology-density relation because the local background density determines the dynamical timescales ( $\tau \propto \rho^{-1/2}$ ), which is closely related to the star formation rates. Elliptical and lenticular galaxies that are likely to be formed in dense environment are assumed to build up their bodies rapidly, due to short dynamical times, without a late accretion phase, whereas spiral galaxies build up their outer parts by accreting intergalactic material after the initial collapse phase. This picture of spiral galaxy formation is in good agreement with the inside-out growth picture of spiral galaxies.

Although the local background density appears to be the primary parameter dictating the morphology of a galaxy, its role is different for giant galaxies and dwarf galaxies. For giant galaxies, the local background density constrains the galaxy morphology through the star formation efficiency in the early phase of galaxy formation. In contrast, the local background density constrains the interaction rates between the host galaxies and their satellites, which are mostly dwarf galaxies because interaction rates are closely related to the orbital period that is determined by the dynamical timescales. Therefore, we suppose

that dEs, dSphs, and dwarf lenticulars, which are likely to be observed in the high-density regions, lose their gas quickly due to frequent interactions with large galaxies. On the other hand, dE<sub>blue</sub> galaxies must have fewer interactions than other dwarf galaxies to keep their gas longer. In the case of the dE<sub>bc</sub>, the role of local background density is twofold. It is high enough for frequent interactions to remove gas from the galaxy but it allows delayed accretion of gas to the nucleus of the dE galaxy to make the blue core.

Most of the local galaxies have nearby companion galaxies. The mean projected distance to the nearest neighbor  $\bar{r}_p$  is  $\sim 260\text{kpc}$ , which is similar to the virial radius of a bright spiral galaxy. Approximately 70% of the local galaxies have the nearest neighbor within  $r_p = \bar{r}_p$ . On the other hand, a considerable number of galaxies are extremely isolated. The number of extremely isolated galaxies depends on the isolation criteria. If  $r_p = 1.5\text{Mpc}$  is taken as the minimum projected separation between a target galaxy and its nearest neighbor, the number of extremely isolated galaxies is 113 but it becomes 66 if we consider  $r_p > 2\text{Mpc}$  as the criterion for the extreme isolation.

The authors are grateful to R.J. Buta, for valuable comments and suggestions which greatly improved this paper. This work was supported by the NRF Research grant 2010-0023319.

## REFERENCES

- Abazajian, K. N., Adelman-McCarthy, J. K., Agueros, M. A., et al. 2009, *ApJS*, 182, 543
- Abraham, R. G., Valdes, F., Yee, H. K. C., & van den Bergh, Sidney, 1994, *ApJ*, 432, 75
- Abraham, R. G., van den Bergh, Sidney, & Nair, P. 2003, *ApJ*, 588, 218
- Aguerri, J. L. A., Iglesias-Paramo, J., Vilchez, J. M., Munoz-Tunon, C., & Sanchez-Janssen, R. 2005, *AJ*, 130, 475
- Ann, H. B., Park, C., & Choi, Y.-Y. 20008, *MNRAS*, 389, 86
- Ann, H. B. 2014, *Journal of the Korean Astronomical Society*, 47, 1.
- Barazza, F. D., Jablonka, P., Desai, V., et al. 2009, *Astronomy and Astrophysics*, 497, 713
- Bernardi, M., Sheth, R. K., Annis, J., et al. 2003, *AJ*, 125, 1849
- Bernardi, M., Meert, A., Vikram, V., et al. 2014, *MNRAS*, 443, 874
- Binggeli, B., Sandage, A., & Tammann, G. A. 1985, *AJ*, 90, 1681
- Binney, J. 1978, *MNRAS*, 183, 501
- Binney, J., & de Vaucouleurs, G. 1981, *MNRAS*, 194, 679
- Boselli, A., Boissier, S., Cortese, L., & Gavazzi, G. 2008, *ApJ*, 674, 742
- Buta, R. J., & Combes, F. 1996, *Fund. Cosmic Physics*, 17, 95
- Buta, R. J., Alpert, A. J., Cobb, M. L., Croker, D. A., & Purcell, G. B. 1998, *AJ*, 116, 1142
- Buta, R. J. 2013, *Planets, Stars and Stellar Systems Vol. 6*, Eds. Oswalt, Terry D., & Keel, William C. (New York: Springer Science+Business Media Dordrecht)

- Buta, R. J., Corwin, H. G., Odewahn, S. C., & Dejaiffe, R. 2007, *The de Vaucouleurs Atlas of Galaxies* (Cambridge: Cambridge University Press)
- Buta, R. J., Sheth, K., Athanassoula, E., et al. 2015, arXiv:150100454
- Cheng, J. Y., Faber, S. M., Simard, L., Graves, G. J., Lopez, E. D., Yan, R., & Cooper, M. C. 2011, *MNRAS*, 412, 727
- Chiboucas, K., Karachentsev, I. D., & Tully, R. B. 2009, *AJ*, 137, 3009
- Cibinel, A., Carollo, C. M., Lilly, S. J., et al. 2013, *ApJ*, 776, 72
- Choi, Y.-Y., Han, D.-H., & Kim, S. S. 2010, *Journal of the Korean Astronomical Society*, 43, 191
- Choi, Y.-Y., Park, C., & Vogeley, M. S. 2007, *ApJ*, 658, 884
- Colless, M. et al. 2001, *MNRAS*, 328, 1039
- Combes, F. 2014, *ASPC*, 480, 211
- Conselice, C. J. 2003, *ApJS*, 147, 1
- Cowie, L. L., Songaila, A., Hu, E., & Cohen, J. G. 1996, *AJ*, 112, 839
- de Vaucouleurs, G. 1959, *Handbuch der Physik*, Volume 53, p.275
- de Vaucouleurs, G., de Vaucouleurs, A., & Corwin, J. R. 1976, *Second Reference Catalogue of Bright Galaxies* (Austin: University of Texas Press)
- de Vaucouleurs, G., de Vaucouleurs, A., Corwin, H. G., Buta, R. J., Paturel, G., & Fouque, P. 1991, *Third Reference Catalogue of Bright Galaxies* (New York: Springer)
- Disney, M., Davies, J., & Phillipps, S. 1989, *MNRAS*, 239, 939

- Dressler, A. 1980, *ApJ*, 236, 351
- Ferguson, H. C., & Binggeli, B. 1994, *Astronomy and Astrophysics Review*, 6, 67
- Geha, M., van der Marel, R. P., Guhathakurta, P., Gilbert, K. W., Kalirai, J., & Kirby, E. N. 2010, *ApJ*, 711, 361
- Gerola, H., & Seiden, P. E. 1978, *ApJ*, 223, 129
- Gil de Paz A., Madore B. F., & Pevunova, O. 2003, *ApJS*, 147, 29
- Gilmore, G., Wilkinson, M. I., Wyse, R. F. G., Kleyna, J. T., Koch, A., Evans, N. W., & Grebel, E. K. 2007, *ApJ*, 663, 948
- Gomez et al. 2003, *ApJ*, 584, 210
- Goto, T., Yamauchi, C., Fujita, Y., Okamura, S., Sekiguchi, M., Smail, I., Bernardi, M., & Gomez, P. L. 2003, *MNRAS*, 346, 601
- Graham, A. W., & Guzman R., 2003, *AJ*, 125, 2936
- Graham, A. W. 2013, in *Planets, Stars and Stellar Systems*, vol. 6, p91-140, eds T. D. Oswalt & W. C. Keel (Springer: Berlin) (arXiv:1108.0997)
- Gu, Q., Zhao, Y., Shi, L., Peng, Z., & Luo, X. 2006, *AJ*, 131, 806
- Gunn, James E., & Gott, J. Richard, III, 1972. *ApJ*, 176, 1
- Guo, Y., McIntosh, D. H., Mo, H. J., Katz, N., van den Bosch, F. C., Weinberg, M., Weinmann, S. M., Pasquali, A., Yang, X. 2009, *MNRAS*, 398, 1129
- Hallenbeck, G., Papastergis, E., Huang, S., Haynes, M. P., Giovanelli, R., Boselli, A., Boissier, S., Heinis, S., Cortese, L., & Fabello, S. 2012, *AJ*, 144, 87

- Heidmann, J., Heidmann, N., & de Vaucouleurs, G. 1972, *Memoirs of the Royal Astronomical Society*, 75, 85
- Hodge, P. W. 1963, *AJ*, 68, 691
- Hodge, P. W. 1973, *ApJ*, 182, 671
- Holmberg, E. 1958, *Lund Medd Astron.. Obs, Ser. II*, 136, 1
- Hubble, E. 1926, *ApJ*, 64, 321
- Hubble, E. 1936, *Realm of the Nebulae* (New Haven: Yale University Press)
- Huertas-Company, M., Rouan, D., Tasca, L., Soucail, G., & Le Fevre, O. 2008, *A&A*, 478, 971
- Jones, H., Davies, J. I., & Trewhella, M. 1996, *MNRAS*, 283, 316
- Jerjen, H., & Binggeli, B. 1997, in *ASP Conf. Ser. 116, The Nature of Elliptical Galaxies; 2nd Stromlo Symposium*, ed. M. Arnaboldi, G. S. Da Costa, and P. Saha (San Francisco, CA: ASP), 239
- Karachentsev, I. D., Nasonova, O. G., & Helene M. 2011, *ApJ*, 743, 123
- Karachentsev, I. D., Makarov, D. I., & Kaisina, E. I. 2013, *AJ*, 141, 101
- Karachentsev, I. D., & Nasonova, O. G. 2013, *MNRAS*, 429, 2677
- Karachentsev, I. D., Nasonova, O. G., & Courtois, H. M. 2013, *MNRAS*, 429, 2264
- Karachentsev, I. D., Karachentseva, V. E., & Nasonova, O. G. 2014, *astro-ph1406.2467*
- Kelly, Brandon C.; McKay, Timothy A. 2004, *AJ*, 127, 625



- Kim, E., Kim, M., Hwang, N., Lee, M. G., Chun, M.-Y., & Ann, H. B. 2011, MNRAS, 411, 1881
- Kormendy, J. 1985, ApJ, 295, 73
- Kormendy, J., & Freeman, K. C. 2014, 2014arXiv1411.2170K (arXiv: 1411 2170)
- Kormendy, J., & Bender, R. 2012 ApJS, 198, 2
- Kormendy, J., Fisher, D. B., Cornell, M. E., & Bender, R. 2009, ApJ, 182, 216
- Kraan-Korteweg, R. C. 1986, Astronomy and Astrophysics Supplement Series , 66, 255
- Kraljic, K., Bournaud, F., & Martig, M. 2012, ApJ, 757, 60
- Kreckel, K., Peebles, P. J. E., van Gorkom, J. H., van de Weygaert, R., & van der Hulst, J. M. 2011, AJ, 141, 204
- Kunth, D. & Ostlin, G. 2000, The Astronomy and Astrophysics Review, 10, 1
- Larson, R. B. 1976, MNRAS, 176, 31
- Lee, G.-H., Woo, J.-H., Lee, M. G., Hwang, H. S., Lee, J. C., Sohn, J., & Lee, J. H. 2012, ApJ, 750, 141
- Lewis, I. et al. 2002, MNRAS, 334, 673
- Lintott, C. J., et al., 2008, MNRAS, 389, 1179
- Lisker T., Glatt K., Westera P., & Grebel E. K. 2006, AJ, 132, 2432
- Lisker T., Grebel E. K., Binggeli B., & Glatt K. 2007, ApJ, 660, 1186
- Lisker, T. 2009, Astronomische Nachrichten, 330, 1043
- Lisker, T., Weinmann, S. M., Janz, J., & Meyer, H. T. 2013, MNRAS, 432, 1162

- Lotz, J. M., Primack, J., & Madau, P. 2004, *AJ*, 128, 163
- Lupton, R., Blanton, M. R., Fekete, G., Hogg, D. W., O’Mullane, W., Szalay, A., & Wherry, N. 2004, *PASP*, 116, 133
- Makarov, D., & Karachentsev, I. 2011, *MNRAS*, 412, 2498
- Matteucci F., & Francois P. 1989, *MNRAS*, 239, 885
- McConnachie, A. W. 2012, *AJ*, 144, 4
- McIntosh, D. H. et al. 2005, *ApJ*, 632, 191
- Michard, R., & Simien, F. 1993 *A&A*, 274, 25
- Michard, R. 1999, *A&AS*, 137, 245
- McIntosh, D. T. et al., 2005, *ApJ*, 632, 191
- Moore B., Katz N., Lake G., Dressler A., & Oemler A. 1996, *Nature*, 379, 613
- Moore B., Lake G., & Katz N. 1998, *ApJ*, 495, 139
- Mould, J. R., Huchra, J. P., Freedman, W. L., et al. 2000, *ApJ*, 529, 786
- Muldrew, S. I., Croton, D. J., Skibba, R. A., et al. 2012, *MNRAS*, 419, 2670
- Nair, P.B., & Abraham, R.G., 2010, *ApJS*, 186, 427
- Naab, T., & Ostriker, J. P. 2006, *MNRAS*, 366, 899
- Oh, S., Oh, K., & Yi, S. K. 2012, *ApJS*, 198, 40
- Pak, M., Rey, S.-C., Lisker, T., Lee, Y., Kim, S., Sung, E.-C., Jerjen, H., Chung, J. 2014, *MNRAS*, 445, 630

- Park, C., & Choi, Y.-Y. 2005, *ApJ*, 635, L29
- Park, C., Choi, Y.-T., Vogeley, M. C., Gott, J., R., & Blanton, M. 2007, *ApJ*, 658, 898
- Park, C., Gott, J., R., & Choi, Y.-Y. 2008, *ApJ*, 674, 784
- Park, C., & Choi, Y.-Y. 2009, *ApJ*, 691, 1828 2002, *MNRAS*, 332, 59
- Peppel, U. C., Drapatz, S., Ghosh, S. K. 1986, *Mitteilungen der Astronomischen Gesellschaft*, 67, 392
- Roychowdhury, S., Chengalur, J. N., Begum, A., Karachentsev, I. D. 2010, *MNRAS*, 404, 60
- Salucci, P., Wilkinson, M. I., Walker, M. G., Gilmore, G. F., Grebel, E. K., Koch, A., Frigerio Matins, C., & Wyse, R. F. G. 2012, *MNRAS*, 420, 2034
- Sancisi, R., Fraternali, F., Oosterloo, T., van der Hulst, T. 2008, *The Astronomy and Astrophysics Review*, 15, 189
- Sandage, A. R. 1961, *The Hubble Atlas of Galaxies* (Washington, DC: Carnegie Institution of Washington)
- Sandage, A., & Bedke, J. 1994, *The Carnegie Atlas of Galaxies* (Washington, DC: Carnegie Institution of Washington)
- Sandage, A., & Binggeli, B. 1984, *AJ*, 89, 919
- Sandage, A., & Tammann, G. A. 1981, *A Revised Shapley-Ames Catalog of Bright Galaxies* (Washington, DC: Carnegie Inst.)
- Sargent, W. L. W., & Searle, L. 1970, *ApJ*, 162, L155
- Scarlata, C., Carollo, C. M., Lilly, S., et al. 2007, *ApJS*, 172, 406

- Schechter, P. 1976, *ApJ*, 203, 297
- Shen, S., Mo, H. J., White, Simon D. M., et al. 2003, *MNRAS*, 343, 978
- Schlegel, D. J., Finkbeiner, D.P., Davis, M. 1988, *ApJ*, 500, 525
- Skibba, R. A., Masters, K. L., Nichol, R. C., et al. 2012, *MNRAS*, 423, 1485
- Stoughton, C., Lupton, R. H., Bernardi, M., et al. 2002, *AJ*, 123, 485
- Strateva, I., Ivezić, Z., Knapp, G. R., et al. 2001, *AJ*, 122, 1861
- Strom, S. E. 1980, *ApJ*, 237, 686
- Suh, H., Jeong, H., Oh, K., Yi, S. K., Ferreras, I., & Schawinski, K. 2010, *ApJS*, 187, 374
- Tanaka, M., Goto, T., Okamura, S., Shimasaku, K., Brinkmann, J. 2004, *AJ*, 128, 2677
- Thuan, T. X., & Martin, G. E. 1981, *ApJ*, 247, 823
- Toloba, E., Boselli, A., Peletier, R. F., Falcon-Barroso, J., van de Ven, G., & Gorgas, J. 2012, *A&A*, 548, 78
- van den Bergh, S. 1960, *ApJ*, 131, 215
- van den Bergh, S. 1976, *ApJ*, 206, 883
- van den Bergh, S. 1988, *PASP*, 100, 344
- van der Hulst, T., & Sancisi, R. 2004, in *IAU Symp. Recycling Intergalactic and Interstellar Matter*, ed. M. Arnaboldi, G. S. Da Costa, O. Saha (San Fransico, CA: ASP), 122
- Walker, M. G., Mateo, M., Olszewski, E. W., Penarrubia, J., Wyn E. N., Gilmore, G. 2009, *ApJ*, 704, 1274
- Walker, M. G. 2013, *Planets, Stars and Stellar Systems Vol. 5*, 1039 (New York: Springer)

- Weijmans, A.-M., de Zeeuw, P. T., Emsellem, E., et al. 2014, MNRAS, 444, 3340
- Weisz, D. R., Dolphin, A. E., Dalcanton, J. J., et al. 2011, ApJ, 743, 8
- White S. D. M., & Rees M. J. 1978, MNRAS, 183, 341
- Willett, K. W., Lintott, C. J., Bamford, S. P., et al. 2013, MNRAS, 435, 2835
- Wirth, A., & Gallagher, J. S., III. 1984, ApJ, 282, 85
- York, D. G., Adelman, J., Anderson, J. E., Jr., et al. 2000, AJ, 120, 1579
- Zwicky, F., & Zwicky, M. A. 1971, Catalogue of Selected Compact Galaxies and of Post-Eruptive Galaxies (Zurich: Offsetdruck L. Speich)